International Journal of General Medicine

Dovepress
Taylor & Francis Group

Open Access Full Text Article

ORIGINAL RESEARCH

A POSTN$^+$ CAF/APOE$^+$ TAM Axis is Associated with Tumor Progression and Potential Immunotherapy Resistance in Laryngeal Squamous Cell Carcinoma

Kexin Ma, Jinqiao Tian, Hao Wu, Shuzheng Wang, Hao-Sheng Ni

Department of Otolaryngology, Affiliated Hospital of Nantong University, Medical School of Nantong University, Nantong, Jiangsu, People's Republic of China

Correspondence: Hao-Sheng Ni, Email entnhs@ntu.edu.cn

Background: Laryngeal squamous cell carcinoma (LSCC) is a prevalent malignancy of the head and neck, characterized by a complex tumor microenvironment (TME) that hinders the effectiveness of immunotherapy.

Objective: This study aimed to comprehensively characterize the features, interactions, and clinical significance of POSTN$^+$ cancer-associated fibroblasts (CAFs) and APOE$^+$ tumor-associated macrophages (TAMs) within the LSCC TME through integrative multi-omics analysis.

Methods: We integrated single-cell RNA sequencing, spatial transcriptomics, and bulk RNA-seq data from the GEO and TCGA databases. Differential expression, functional enrichment, cell–cell communication, multiplex immunofluorescence, spatial colocalization, molecular docking, and survival analyses were performed, with independent validation in the IMvigor210 immunotherapy cohort.

Results: A total of 206,399 cells were obtained from 29 LSCC single-cell samples (Tumor=16, Normal=13) and POSTN$^+$ CAF/APOE$^+$ TAM gene sets were identified. POSTN$^+$ CAFs and APOE$^+$ TAMs were enriched in LSCC tissues, and associated with epithelial–mesenchymal transition (EMT) and M2 macrophage polarization, respectively. Cell–cell communication and spatial analyses revealed close bidirectional signaling and spatial colocalization between the two cell types. Multiplex immunofluorescence staining further confirmed their close spatial proximity. Molecular docking suggested a potential structural compatibility between POSTN and APOE. Bulk RNA-seq analysis showed that their co-enrichment correlated with poor prognosis and resistance to immunotherapy, which were further confirmed in pan-cancer datasets.

Conclusion: The POSTN$^+$CAF/APOE$^+$TAM axis is cooperatively associated with aggressive tumor behavior in LSCC and shapes an immunosuppressive microenvironment. This cellular axis may serve as a potential biomarker and therapeutic target for predicting prognosis and responsiveness to immunotherapy in LSCC.

Keywords: laryngeal squamous cell carcinoma, tumor microenvironment, POSTN, APOE, cancer-associated fibroblast, tumor-associated macrophage

Introduction

Laryngeal squamous cell carcinoma (LSCC) is one of the most frequent malignancies in the head and neck, while its morbidity and mortality are increasing.[1,2] Although the treatment of surgery, radiotherapy, and chemotherapy has made some progress in LSCC, the five-year survival rate of advanced or recurrent LSCC is still unsatisfied.[3] Immunotherapy, especially immune checkpoint inhibitors (ICIs), has provided novel hope for the treatment of LSCC in recent years. Nonetheless, the response rate is restricted, and some patients gain very little benefit.[4] The complexity of the tumor microenvironment (TME) is one major cause for this restricted efficacy.[5] It is well accepted that the TME, consisting of tumor and stromal cells, immune cells, and extracellular matrix (ECM) components, is a complex environment that actively participates in the initiation and progression of tumors through invasion, metastasis, and drug resistance.[6]

https://doi.org/10.2147/IJGM.S583478
Received: 4 December 2025
Accepted: 21 April 2026
Published: 3 May 2026

Among the stromal components in the TME, cancer-associated fibroblasts (CAFs) and tumor-associated macrophages (TAMs) are among the most abundant and functionally important.[7] CAFs secrete growth factors and cytokines, remodeling the extracellular matrix (ECM), to support the growth, invasion, and angiogenesis of tumor cells.[8,9] TAMs, frequently polarized to an M2-like phenotype, foster an immunosuppressive microenvironment by suppressing T-cell activity, promoting angiogenesis, and aiding tissue remodeling.[10–12] However, CAFs and TAMs are functionally highly heterogeneous. At different stages of tumor progression, they are defined by diverse subpopulations that play opposing or divergent roles.[13,14] Thus, it is critical to define the phenotypic features and crosstalk networks of these important stromal subtypes at a high resolution level for unraveling tumor etiology and drug targets. Recent developments in single-cell RNA sequencing (scRNA-seq) techniques greatly facilitate the thorough characterization of cellular composition and transcriptional states at a single-cell resolution.[15] This technique allows precise identification of diverse cell subpopulations within the TME and reveals their unique transcriptional and functional signatures, particularly those of CAFs and TAMs. In addition to constructing comprehensive cell atlases, scRNA-seq could also be used to identify complex intercellular communication networks, thus offering a promising paradigm in the discovery of the novel therapeutic targets.[16]

POSTN (periostin) is a secretory ECM protein that is critically involved in tissue repair, fibrosis, and tumor progression.[17] In various cancers, POSTN is primarily synthesized by CAFs and shows a positive correlation with increased tumor invasiveness, metastasis, and unfavorable clinical prognosis.[18–21] As a vitally important lipoprotein in the body, apolipoprotein E (APOE) plays a crucial role as both a lipid carrier and lipid transporter,[22] which is involved in immune responses within the tumor microenvironment.[23] APOE is predominantly expressed by TAMs and linked to M2-like macrophages, which are immunosuppressive cells. Its upregulation is found to promote immune evasion, leading to immunotherapy resistance.[4]

Although $POSTN^+$ CAFs and $APOE^+$ TAMs have been reported in multiple cancer types, their specific characteristics, potential crosstalk, and combined clinical significance in LSCC remain unclear. We hypothesized that $POSTN^+$ CAFs and $APOE^+$ TAMs form a cooperative stromal–immune axis that is associated with tumor progression, immune suppression, and potential immunotherapy resistance in LSCC. Based on this hypothesis, we integrated scRNA-seq, spatial transcriptomics, and bulk RNA-seq data to systematically characterize the molecular features, spatial relationships, interaction patterns, and clinical relevance of these two cell populations in the LSCC tumor microenvironment.

Materials and Methods

Data Sources

This study employed single-cell RNA sequencing (scRNA-seq) data of laryngeal squamous cell carcinoma (LSCC) sourced from the GEO database (GSE206332, GSE252490, and GSE290927), alongside transcriptomic and clinical follow-up data from The Cancer Genome Atlas (TCGA) for analysis and validation (https://xenabrowser.net/datapages/). Spatial transcriptomics (GSE181300), generated using the 10x Genomics platform, were also retrieved from GEO. For pan-cancer validation, scRNA-seq datasets were collected from GEO, including GSE155698 (pancreatic ductal adenocarcinoma, PDAC), GSE159115 (renal cell carcinoma, RCC), GSE149614 (liver hepatocellular carcinoma, LIHC), GSE166555 (colorectal cancer, CRC), GSE184880 (ovarian cancer, OVCA), GSE138709 (intrahepatic cholangiocarcinoma, ICC), GSE181294 (prostate adenocarcinoma, PRAD), GSE131907 (lung adenocarcinoma, LUAD), GSE180286 (breast invasive carcinoma, BRCA), GSE181919 (head and neck squamous cell carcinoma, HNSC), and GSE163558 (gastric cancer, GC). Bulk RNA-seq datasets (GSE41613 and GSE65858, both HNSC) were also obtained from GEO. The IMvigor210 cohort was accessed through the IMvigor210CoreBiologies R package and was used as an exploratory external immunotherapy-treated dataset, because publicly available LSCC cohorts with matched transcriptomic profiles and immunotherapy response data remain limited. Protein sequence and structural data were retrieved from the UniProt database (https://www.uniprot.org/). Considering the limited sample size of laryngeal squamous cell carcinoma in TCGA-LSCC (n=123, tumor=111, normal=12) and the fact that LSCC is a representative subgroup of HNSC, we further validated the results in TCGA-HNSC (n=566, tumor=522, normal=44) to ensure consistency of the results.

This study was approved by the Ethical Committee of the Affiliated Hospital of Nantong University (2023-K091-01) and was conducted in accordance with the Declaration of Helsinki. Tumor tissues from patients with laryngeal squamous cell carcinoma were obtained from surgical resections performed at the Affiliated Hospital of Nantong University. Written informed consent was obtained from all enrolled patients.

Single-Cell Data Analysis

Seurat (v4.3.0) was used to examine data from single-cell RNA sequencing (scRNA-seq).[24] After data import and cross-sample merging, quality control was performed based on the following criteria: mitochondrial gene proportion <20%, UMI count >500, and identified genes >200. The qualified cells were normalized using the NormalizeData function, and the genes with high variability were identified using FindVariableFeatures. RunPCA was used to reduce dimensionality, while Harmony (v0.1.0) was utilized to account for batch effects. Cell clustering was performed using FindNeighbors and FindClusters (resolution = 0.1), with the results visualized using UMAP. DecontX (contamination threshold < 0.2)[25] was used to remove ambient RNA contamination. Canonical marker genes from previous studies were used to annotate cell clusters. Using the FindMarkers method and the Wilcoxon rank-sum test, differentially expressed genes (DEGs) were identified using the criterion $|\log_2 FC| > 0.25$ and FDR < 0.05.

Functional Enrichment Analysis

ClusterProfiler (v4.10.1)[26] was used to carry out functional annotation and pathway enrichment analyses of DEGs, referencing the Gene Ontology (GO) and Kyoto Encyclopedia of Genes and Genomes (KEGG) databases. Statistical significance was established at FDR < 0.05. The GSVA (v1.50.5) package[27] was used to score pathway activity using the single-sample gene set enrichment analysis (ssGSEA) approach, with the MSigDB database's Hallmark, KEGG, and Reactome gene sets as references.

Pseudo Time Trajectory Analysis

Monocle2 (v2.30.1) was used to analyze the developmental pathway of cells.[28] Highly variable genes were chosen as ordering features, and dimensionality reduction was performed using the DDRTree algorithm to rebuild the trajectory, inferring the dynamic transcriptional transitions of cells throughout tumor progression.

Cell-to-Cell Communication Analysis

CellChat (v2.2.0) was used to examine intercellular signaling connections.[29] Low-abundance cell clusters were filtered with a minimum cell count of 10. The interaction intensity of ligand-receptor pairings was calculated using the combined expression levels of the associated genes, and communication networks were displayed using the netVisual_circle and netVisual_bubble algorithms.

Analysis of Ro/e Enrichment

The observed-to-expected ratio (Ro/e) was calculated to find out the degree to which certain cell subpopulations were enriched in different tissue contexts (tumor vs. normal).[30] The anticipated value was calculated using the total cell count and the overall ratio of each subpopulation. We determined the P values and 95% confidence intervals using either a binomial test or a permutation method. The Ro/e values are categorized as follows: +++, Ro/e > 2.5; ++, 2 < Ro/e ≤ 2.5; +, 1.5 < Ro/e ≤ 2; ±, 1 < Ro/e ≤ 1.5. This analysis was utilized to assess the distributional bias of fibroblast and macrophage subtypes across various tissue microenvironments.

Analysis of Immune Infiltration

Using TCGA bulk RNA-seq data, the ESTIMATE algorithm[31] was employed to compute ImmuneScore, StromalScore, and ESTIMATEScore, as well as to estimate the purity of the tumor. The IOBR package[32] was used to measure immune cell infiltration. It combined four well-known deconvolution algorithms—EPIC,[33] MCP_counter,[34] Quanti-seq,[35] and TIMER[36]—with the ssGSEA method,[27] which is based on immune cell–specific gene signatures. The

Immunophenoscore (IPS) evaluated tumor immunogenicity, whereas immune evasion and potential responsiveness to immune checkpoint inhibitors (ICIs) were forecasted utilizing the TIDE algorithm (http://tide.dfci.harvard.edu/).[37]

Analysis of Survival

We used the survival (v3.8–3) and survminer (v0.5.0) packages to make Kaplan–Meier survival curves and the Log-rank test to see if the results were statistically significant.

Analysis of Spatial Transcriptomics

Spatial transcriptomics underwent preprocessing in Seurat, succeeded by cell type deconvolution utilizing the RCTD (Robust Cell Type Decomposition) algorithm. We used annotated single-cell RNA-seq data as a reference to make a Reference object. Then, we used the spatial expression matrix to figure out what the dominant cell type was for each spatial spot. We used the ssGSEA method to determine the marker genes of fibroblasts and macrophages and then calculated spatial enrichment scores. The results were shown on tissue sections. We explored the spatial correlation between $POSTN^+$ CAFs and $APOE^+$ TAMs by calculating GSVA scores for both cell types and performing Spearman correlation analysis. The results were shown as scatter plots to show the extent to which they were spatially co-localized.

Molecular Docking Analysis

Protein-protein docking was performed with the HDOCK server (http://hdock.phys.hust.edu.cn/), which combines template-based and ab initio hybrid docking strategies. A total of 100 potential binding conformations were created and ranked using iterative knowledge-based scoring functions (ITScorePP or ITScorePR). The conformation with the lowest docking score was chosen as the best model because lower scores usually mean that the binding interaction is more stable and favorable. Protein sequences and structural data for APOE (UniProt ID: P02649) and POSTN (UniProt ID: Q15063) were obtained from the UniProt database. The top-ranked docking complex was visualized and analyzed using PyMOL (v3.0.3, https://pymol.org/) to explore hydrogen bonding and spatial conformations, while LigPlot+ (https://www.ebi.ac.uk/thornton-srv/software/LigPlus/) was used to generate two-dimensional interaction diagrams illustrating hydrogen bonds, hydrophobic contacts, and polar residue interactions.

Multiplex Immunofluorescence

Formalin-fixed, paraffin-embedded tumor tissue sections underwent deparaffinization, rehydration, and antigen retrieval, subsequently followed by blocking with 5% BSA. Sections were then incubated with primary antibodies against POSTN (Epizyme Biotech, catalog number: R014951) and APOE (Epizyme Biotech, catalog number: R013930), followed by FITC- and Cy3-conjugated secondary antibodies. Nuclei were counterstained with DAPI (4',6-diamidino-2-phenylindole). Images were acquired using a Zeiss LSM880 confocal microscope, and colocalization analysis was performed with the Coloc2 plugin in ImageJ.

Statistical Analysis

All statistical analyses were conducted in R (v4.3.1). Differences between two groups were assessed using the Wilcoxon rank-sum test or Kruskal–Wallis test, and comparisons among multiple groups were performed using ANOVA. Correlation analyses were performed using the Pearson or Spearman method as appropriate. Statistical significance was defined as $P < 0.05$.

Results

Single-Cell Transcriptomic Profiling Reveals the Cellular Composition of the LSCC Tumor Microenvironment

A flow diagram of the study is presented in Figure 1A.

To systematically analyze the tumor microenvironment (TME) of LSCC, we combined scRNA-seq profiles of 16 laryngeal cancer and 13 non-cancerous tissue specimens across three independent datasets (GSE206332, GSE252490,

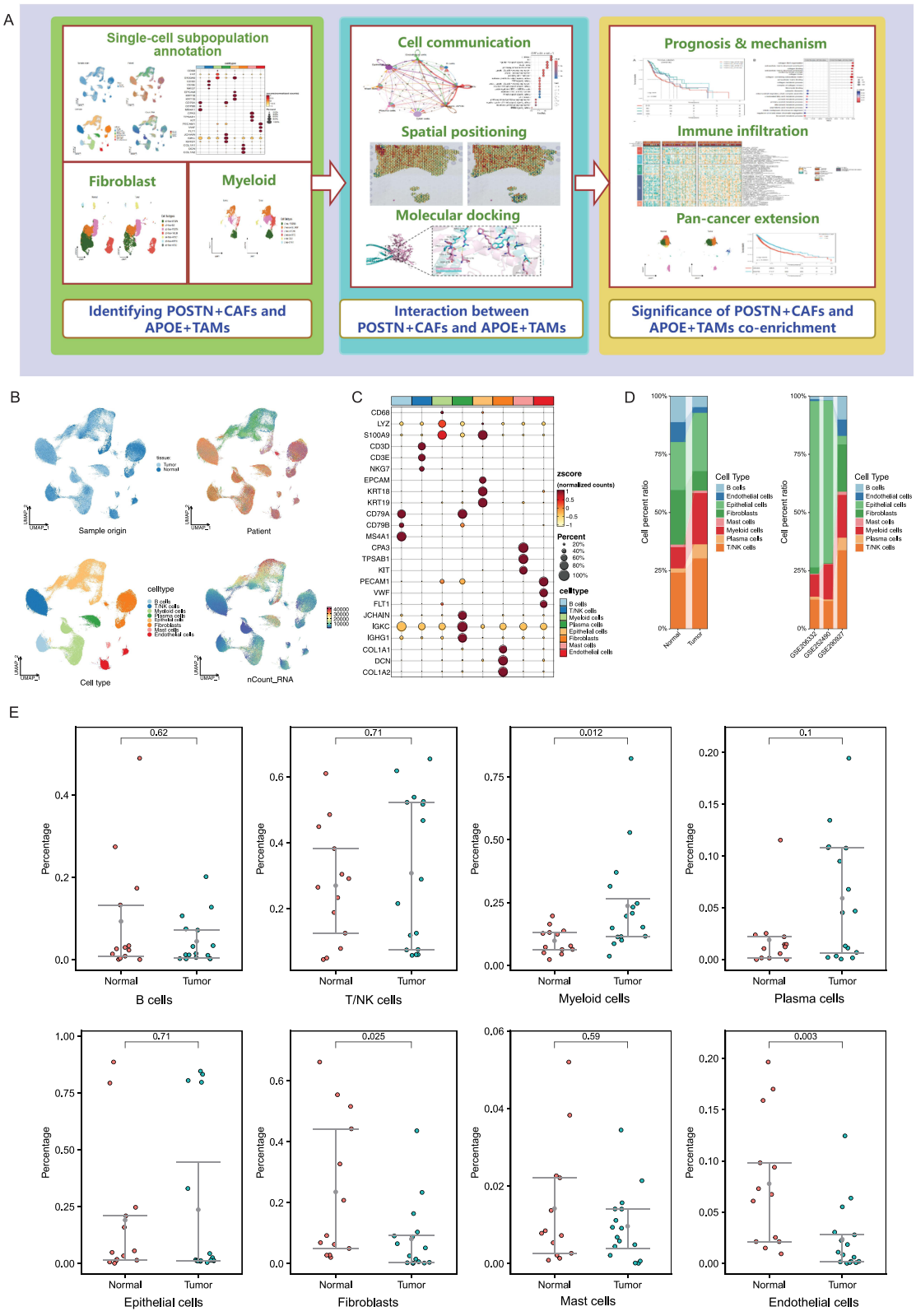

Figure 1 Single-cell transcriptomic landscape of LSCC. (**A**) Study flowchart. (**B**) UMAP visualization of integrated single-cell transcriptomes from LSCC tumor and adjacent normal tissues, colored by sample origin, patient, and annotated cell types. (**C**) Dot plot showing expression patterns of canonical marker genes across major cell types (dot size indicates percentage of expressing cells; color indicates scaled expression). (**D**) Proportions of cell types in tumor vs. normal tissues and across datasets. (**E**) Comparison of cell-type fractions between tumor and normal tissues based on a two-sided Wilcoxon test. Fibroblasts and myeloid cells exhibit significantly altered abundance between tumor and normal conditions.

Abbreviations: UMAP, Uniform Manifold Approximation and Projection; LSCC, laryngeal squamous cell carcinoma.

https://doi.org/10.2147/IJGM.S583478

GSE290927). After stringent quality control, 206,399 cells were kept for further analysis. Unsupervised clustering and annotation based on canonical marker genes described in published literature (Figure 1C) revealed eight main cell types, including B cells, T/NK cells, myeloid subsets, plasma cells, epithelial cells, fibroblasts, mast cells, endothelial cells. UMAP (Uniform Manifold Approximation and Projection) visualization indicated a distinct clustering of these populations, with evident transcriptional alterations and compositional differences in tumor vs. normal tissues as well as between different datasets (Figure 1B). The relative proportions of various cell types were quite heterogeneous in malignant samples from different datasets and origins (Figure 1D). We observed significant distinctions in the compositions of fibroblasts and myeloid cells between tumor and normal tissue (Figure 1E), thereby implicating that these two cell types may be involved with TME remodeling.

$POSTN^+$ CAFs are Associated with LSCC Malignant Progression Through the Induction of EMT

Due to the significant changes in fibroblast populations within tumor tissues, we isolated this cell type for subsequent subclustering analysis. The fibroblasts were categorized into seven transcriptionally distinct subpopulations, identified as c0-fibro-MFAP4, c1-fibro-IL6, c2-fibro-POSTN, c3-fibro-TAGLN, c4-fibro-APOC1, c5-fibro-KRT13, and c6-fibro-APOD (Figure 2A), each distinguished by specific marker genes (Figure 2B). The Ro/e enrichment analysis indicated that the c2-fibro-POSTN subset was markedly enriched in tumor tissues (Figure 2C), implying it constitutes a tumor-specific fibroblast population, identified as $POSTN^+$ cancer-associated fibroblasts (CAFs). Pseudotime trajectory analysis showed that $POSTN^+$ CAFs were at the middle to late stage of fibroblast differentiation (Figure 2D). This suggests that they were in an activated or mature state that may be linked to tumor growth. The top 30 differentially expressed genes (adjusted P value < 0.05) in $POSTN^+$ CAFs constituted the $POSTN^+$ CAF gene set (Supplementary Table 1). This gene set was used to map to the bulk RNA-seq data so that the ssGSEA method can be used to find out how many $POSTN^+$ CAFs are in each sample.

The ssGSEA pathway enrichment analysis indicated that this subgroup demonstrated significantly heightened activity in pro-tumorigenic signaling pathways, such as EMT, angiogenesis, and immune suppression (Figure 2E), aligning with the functional enrichment results of differentially expressed genes (Supplementary Figure 1A–D). EMT is an important biological process that enables epithelial-derived tumor cells to become migratory and invasive.[38] This means that $POSTN^+$ CAFs may help LSCC progress by secreting POSTN and causing EMT in tumor cells.

In the TCGA-LSCC cohort, the prevalence of $POSTN^+$ CAFs was higher in tumor tissues than in normal tissues (Figure 2F). Kaplan–Meier survival analysis indicated that patients with elevated $POSTN^+$ CAFs infiltration demonstrated markedly inferior overall survival (Figure 2G). In the TCGA-HNSC cohort, we obtained identical results (Supplementary Figure 3A and B). These findings collectively designate $POSTN^+$ CAFs as a pivotal pro-tumorigenic element within the LSCC tumor microenvironment, potentially facilitating tumor invasion and metastasis via epithelial-mesenchymal transition (EMT) activation, thereby leading to unfavorable clinical outcomes.

$APOE^+$ TAMs are Associated with LSCC Progression Through M2 Polarization

Similarly, we performed subclustering analysis on myeloid cells and identified 6 distinct subpopulations, including c0-neu-FCGR3B (neutrophils), c1-macro-SELENOP (macrophages), c2-mono-VCAN (monocytes), c3-macro-APOE (macrophages), c4-dc-CCL5 (dendritic cells), and c5-dc-STMN1 (dendritic cells) (Figure 3A). Marker genes for each subcluster are shown in Figure 3B. Ro/e enrichment analysis revealed that the c3-macro-APOE subset was significantly enriched in tumor tissues (Figure 3C), suggesting it represents a tumor-specific macrophage population, hereafter referred to as $APOE^+$ tumor-associated macrophages (TAMs). Pseudotime trajectory analysis described the differentiation path of myeloid cells from monocytes to macrophages, with $APOE^+$ TAMs positioned at the terminal stage (Figure 3D), indicating that they represent a terminally differentiated macrophage state within the TME. The top 30 differentially expressed genes (adjusted P value < 0.05) in $APOE^+$ TAMs constituted the $APOE^+$ TAM gene set (Supplementary Table 2), which was used to map to the bulk RNA-seq data for calculating the abundance of $APOE^+$ TAMs by the ssGSEA method in each sample.

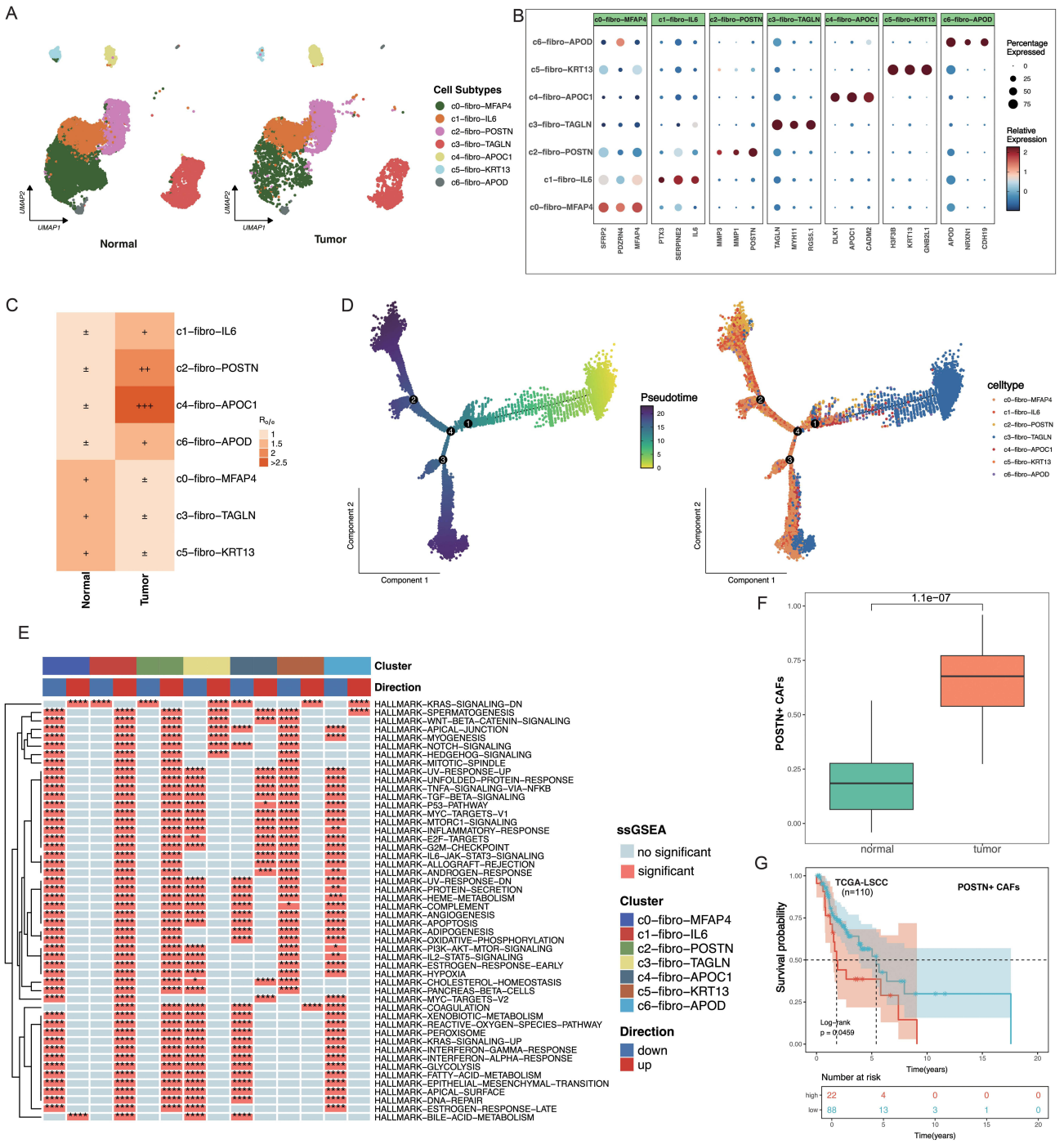

Figure 2 Molecular and functional characterization of fibroblast subpopulations in LSCC. (**A**) UMAP clustering of fibroblasts identifies 7 subpopulations (c0–c6) in LSCC tumor and normal tissues. (**B**) Dot plot showing canonical marker genes defining each fibroblast subtype (dot size: percentage of expressing cells; color: scaled expression). (**C**) Ro/e enrichment analysis comparing tumor versus normal tissues indicates a significant tumor-specific enrichment of c2-fibro-POSTN cells. The Ro/e values are categorized as follows: + ++, Ro/e > 2.5; ++, 2 < Ro/e ≤ 2.5; +, 1.5 < Ro/e ≤ 2; ±, 1 < Ro/e ≤ 1.5. (**D**) Pseudotime trajectory suggests that POSTN$^+$ fibroblasts occupy a late differentiation state. (**E**) ssGSEA analysis demonstrates that POSTN$^+$ fibroblasts exhibit increased activation of pro-tumorigenic pathways, including EMT, angiogenesis, and immunosuppression. *, P<0.05;**, P<0.01; ***,P<0.001;****<0.0001. (**F**) Quantification of POSTN$^+$ CAF abundance in the TCGA-LSCC cohort shows significantly higher levels in tumors than normal tissues (Wilcoxon test). (**G**) Kaplan–Meier curves reveal poorer overall survival in LSCC patients with high POSTN$^+$ CAF infiltration (Log-rank test).

Abbreviations: CAF, cancer-associated fibroblast; EMT, epithelial–mesenchymal transition; LSCC, laryngeal squamous cell carcinoma.

https://doi.org/10.2147/IJGM.S583478

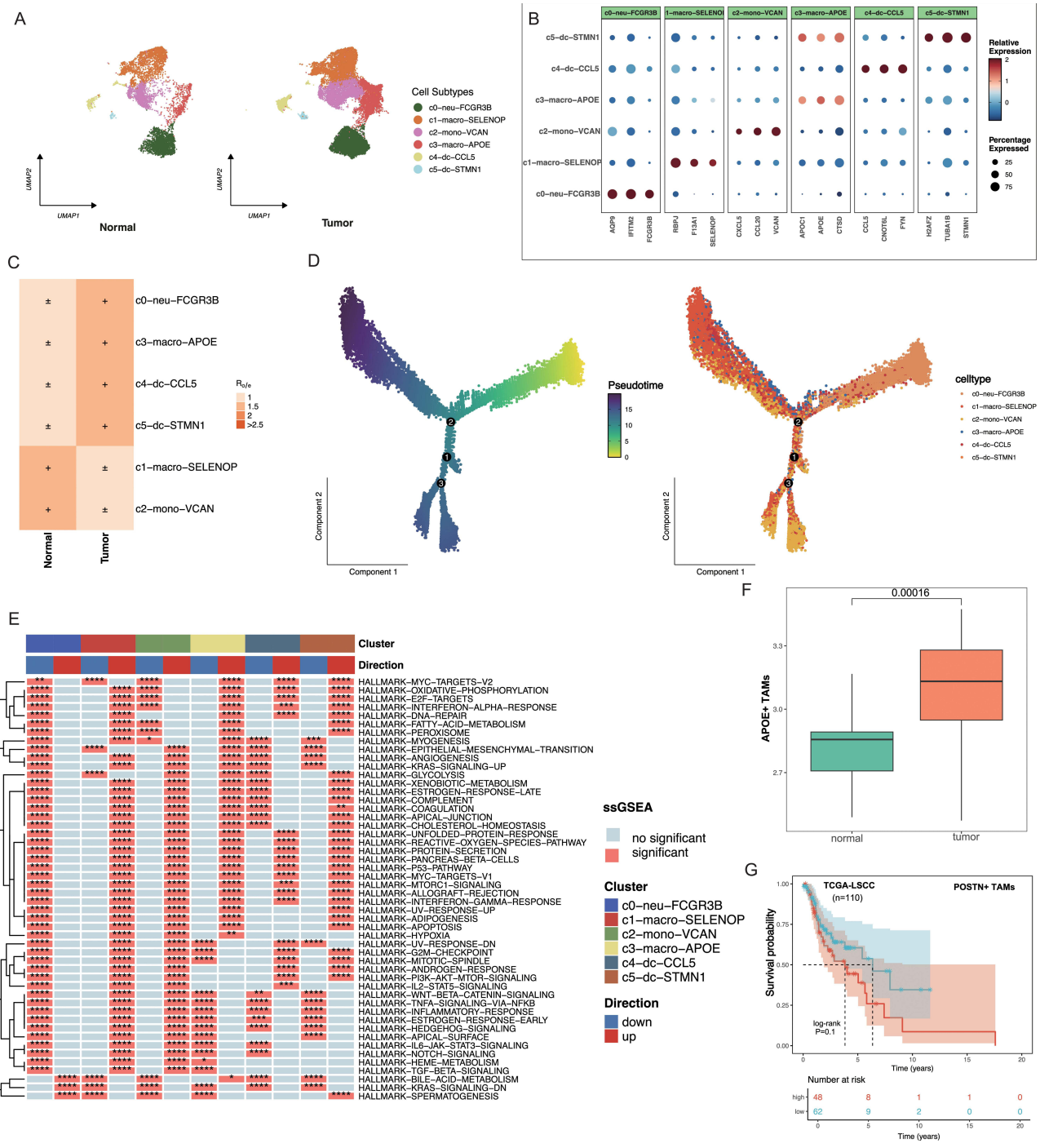

Figure 3 Characterization and functional states of myeloid cell subpopulations in LSCC. (**A**) A UMAP visualization shows six myeloid subclusters in LSCC. (**B**) Dot plot presents representative marker genes for each subcluster. (**C**) Ro/e analysis indicates that APOE$^+$ TAMs are markedly enriched in tumor tissues. The following scale indicates the levels of Ro/e: +, 1.5 < Ro/e ≤ 2; ±, 1 < Ro/e ≤ 1.5. (**D**) Pseudotime trajectory shows that APOE$^+$TAMs occupy a late-stage differentiation state. (**E**) ssGSEA reveals enhanced hypoxia, glycolysis, and immunosuppressive pathways in APOE$^+$TAMs. *, P<0.05;**, P<0.01; ***,P<0.001;****<0.0001. (**F**) The TCGA-LSCC cohort confirms higher abundance of APOE$^+$TAMs in tumors versus normal tissues (Wilcoxon test). (**G**) Kaplan–Meier curves show that high APOE$^+$TAMs levels are associated with poorer overall survival (Log-rank test) in LSCC.

Abbreviations: UMAP, Uniform Manifold Approximation and Projection; LSCC, laryngeal squamous cell carcinoma; TAM, tumor-associated macrophage.

ssGSEA analysis revealed that APOE$^+$ TAMs displayed enhanced activity in hypoxia, glycolysis, and immunosuppressive pathways (Figure 3E), while differentially expressed genes' enrichment analysis confirmed their strong association with M2-like polarization (Supplementary Figure 2A–D). M2-polarized macrophages are well-recognized pro-tumor cells that suppress antitumor immunity and promote tumor growth and angiogenesis.[39]

In the TCGA-LSCC validation cohort, the abundance of APOE$^+$ TAMs was markedly higher in tumor tissues than in normal tissues (Figure 3F), which is consistent with the results in the TCGA-HNSC cohort (Supplementary Figure 3C). Although Kaplan–Meier analysis did not reach statistical significance in LSCC (Figure 3G), patients with high APOE$^+$ TAM infiltration exhibited a trend toward poorer survival in HNSC (Supplementary Figure 3D). Although APOE$^+$ TAM abundance was significantly elevated in LSCC tissues, its association with overall survival in the TCGA-LSCC cohort did not reach statistical significance, whereas a trend toward worse survival was observed in the broader TCGA-HNSC cohort. Together, these findings identify APOE$^+$ TAMs as a key immunosuppressive macrophage population in LSCC that likely promotes tumor progression by establishing an M2-polarized, immunosuppressive microenvironment.

POSTN$^+$ Fibroblasts and APOE$^+$ Macrophages Exhibit Robust Reciprocal Interactions

After identifying POSTN$^+$ CAFs and APOE$^+$ TAMs, we next explored their potential crosstalk using CellChat analysis. The findings demonstrated a robust bidirectional communication network between these two subpopulations (Figure 4A–C).

POSTN$^+$ CAFs predominantly transmitted MIF–(CD74+CD44) and ANXA1–FPR3 ligand–receptor signals to APOE$^+$ TAMs (Figure 4D), both of which are strongly associated with chemotactic signaling and intercellular regulation (Figure 4E), involving cytokine–receptor interactions, complement and coagulation cascades, and efferocytosis pathways (Figure 4F). On the other hand, APOE$^+$ TAMs sent signals back to POSTN$^+$ CAFs mostly through NAMPT–(ITGA5 +ITGB1) and PPIA–BSG interactions (Figure 4G), which are involved in chemotaxis and controlling apoptosis (Figure 4H). Pathway enrichment further underscored the activation of the PI3K–Akt and proteoglycans within cancer pathways (Figure 4I). These results indicate that POSTN$^+$ CAFs and APOE$^+$ TAMs establish a mutually reinforcing positive feedback loop within the tumor microenvironment (TME).

To confirm this interaction spatially, we analyzed spatial transcriptomics from three HNSC samples (GSE181300). In sample GSM5494475, single-cell annotations were positioned on tissue sections (Figure 5A), illustrating the spatial distribution of POSTN$^+$ CAFs and APOE$^+$ TAMs in relation to POSTN and APOE expression (Figure 5B). GSVA scoring showed that these two populations were strongly spatially co-enriched in tumor regions (Figure 5C), and their GSVA scores had a strong positive correlation (R = 0.31, $P < 2.2e{-}16$) (Figure 5D). Similar outcomes were replicated in samples GSM5494476 (Figure 5E–H) and GSM5494479 (Figure 5I–L).

These findings demonstrate that POSTN$^+$ CAFs and APOE$^+$ TAMs are spatially co-localized within LSCC tissues and functionally collaborate, establishing a synergistic interaction network that likely enhances tumor progression and immune suppression.

POSTN$^+$ CAFs are Positively Correlated with APOE$^+$ TAMs and Colocalize Within the Tumor Stroma

To further verify the spatial and quantitative relationship between POSTN$^+$ CAFs and APOE$^+$ TAMs, we conducted cross-cohort correlation analysis (TCGA, GSE41613, and GSE65858) in HNSC and multiplex immunofluorescence staining in LSCC. Most intriguingly, there was a strong positive correlation between the estimated abundance of POSTN$^+$ CAFs and APOE$^+$ TAMs across all three cohorts (R = 0.256–0.509, $P < 0.001$; Figure 6A–C), suggesting an orchestrated pattern of enrichment in the TME.

Their close spatial proximity was also validated by multiplex immunofluorescence staining on LSCC sections. As described in Figure 6D, POSTN (red) and APOE (green) had overlapping localization within the tumor stroma, thus generating mixed regions. These collective results strongly suggest that POSTN$^+$ CAFs and APOE$^+$ TAMs are not only transcriptionally associated but also physically co-localized in this cancer stroma, which is consistent with the notion that they may functionally cooperate to drive tumor progression.

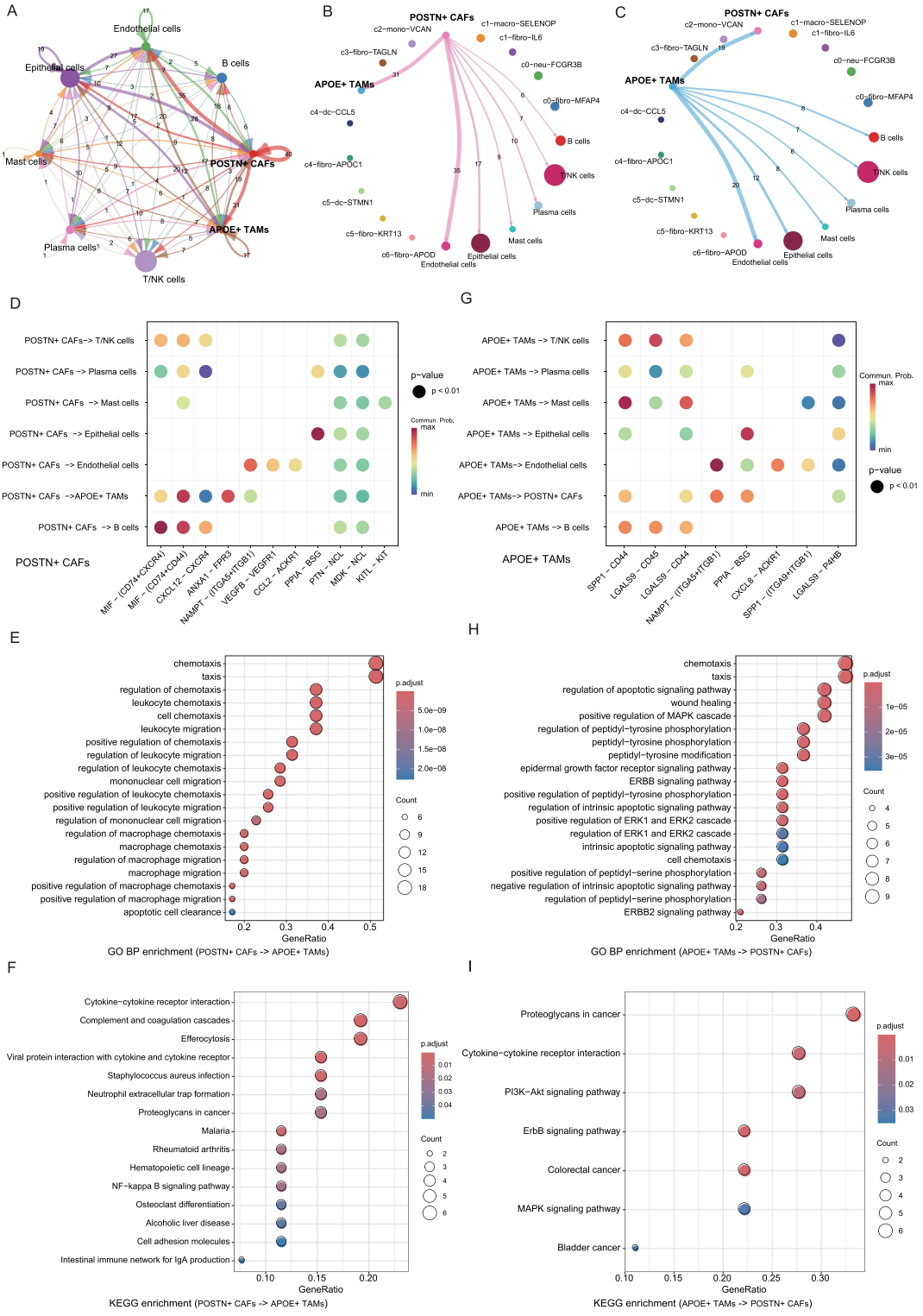

Figure 4 Intercellular communication between POSTN$^+$ CAFs and APOE$^+$ TAMs in LSCC. (**A**) Global ligand–receptor interaction networks reveal strong bidirectional communication between POSTN$^+$ CAFs and APOE$^+$ TAMs. (**B**) Outgoing signaling patterns from POSTN$^+$ CAFs. (**C**) Outgoing signaling patterns from APOE$^+$ TAMs. (In figure A-C, the numbers on the edges indicate the amount of inferred significant intercellular interactions between cell populations.) (**D**) Bubble plots highlight significant ligand–receptor pairs mediating communication from POSTN$^+$ CAFs. (**E**) GO enrichment indicates chemotaxis and apoptotic signaling modulation as major biological processes (from POSTN$^+$ CAFs to APOE$^+$ TAMs). (**F**) KEGG analysis identifies cytokine-cytokine receptor interactions, complement/coagulation as dominant pathways (from POSTN$^+$ CAFs to APOE$^+$ TAMs). (**G**) Bubble plots highlight significant ligand–receptor pairs mediating communication from APOE$^+$ TAMs. (**H**) GO enrichment indicates chemotaxis and apoptotic signaling modulation as major biological processes (from APOE$^+$ TAMs to POSTN$^+$ CAFs). (**I**) KEGG analysis identifies proteoglycans in cancer, cytokine-cytokine receptor interaction as dominant pathways (from APOE$^+$ TAMs to POSTN$^+$ CAFs).

Abbreviations: LSCC, laryngeal squamous cell carcinoma; CAF, cancer-associated fibroblast; TAM, tumor-associated macrophage.

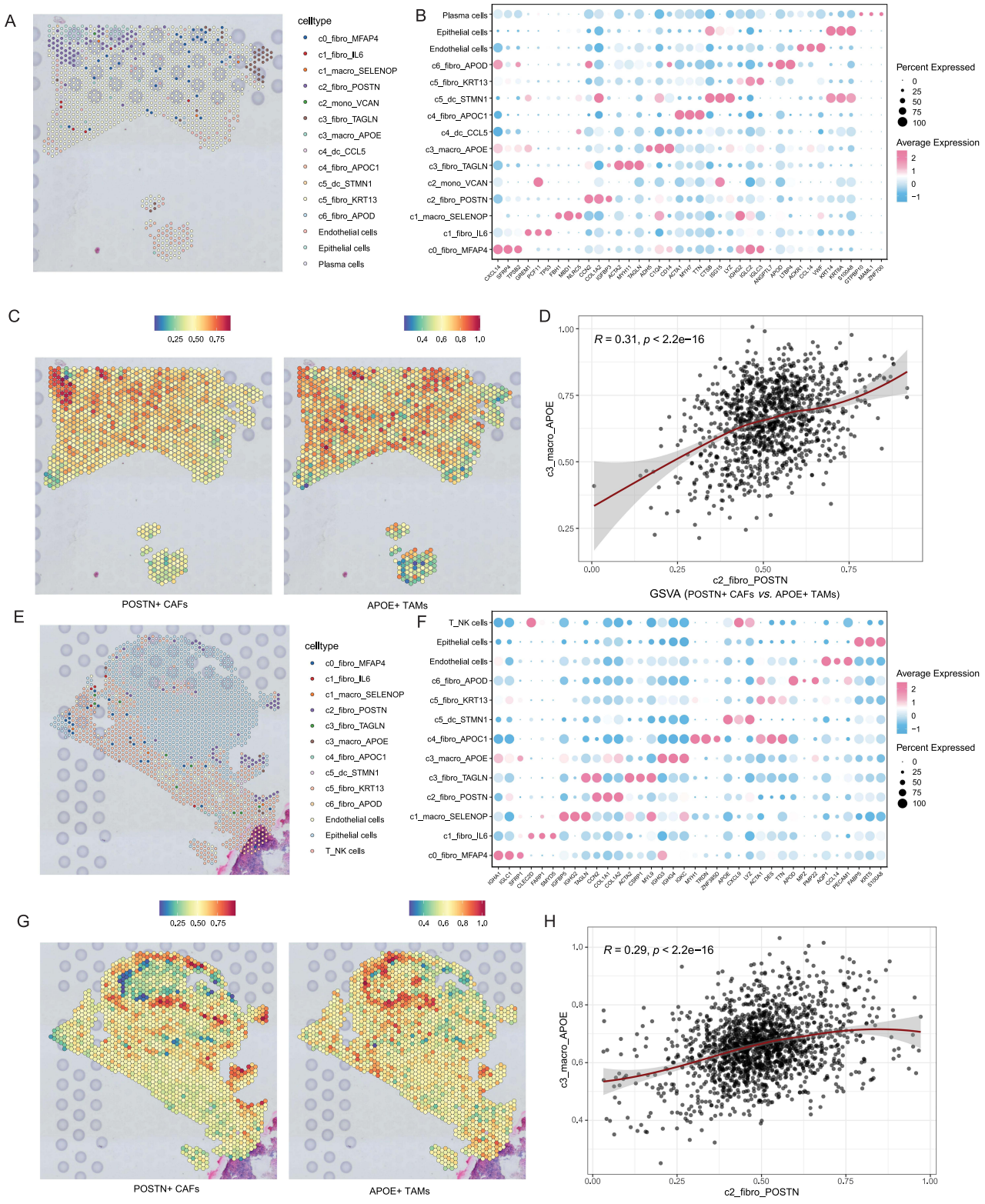

Figure 5 Continued.

https://doi.org/10.2147/IJGM.S583478

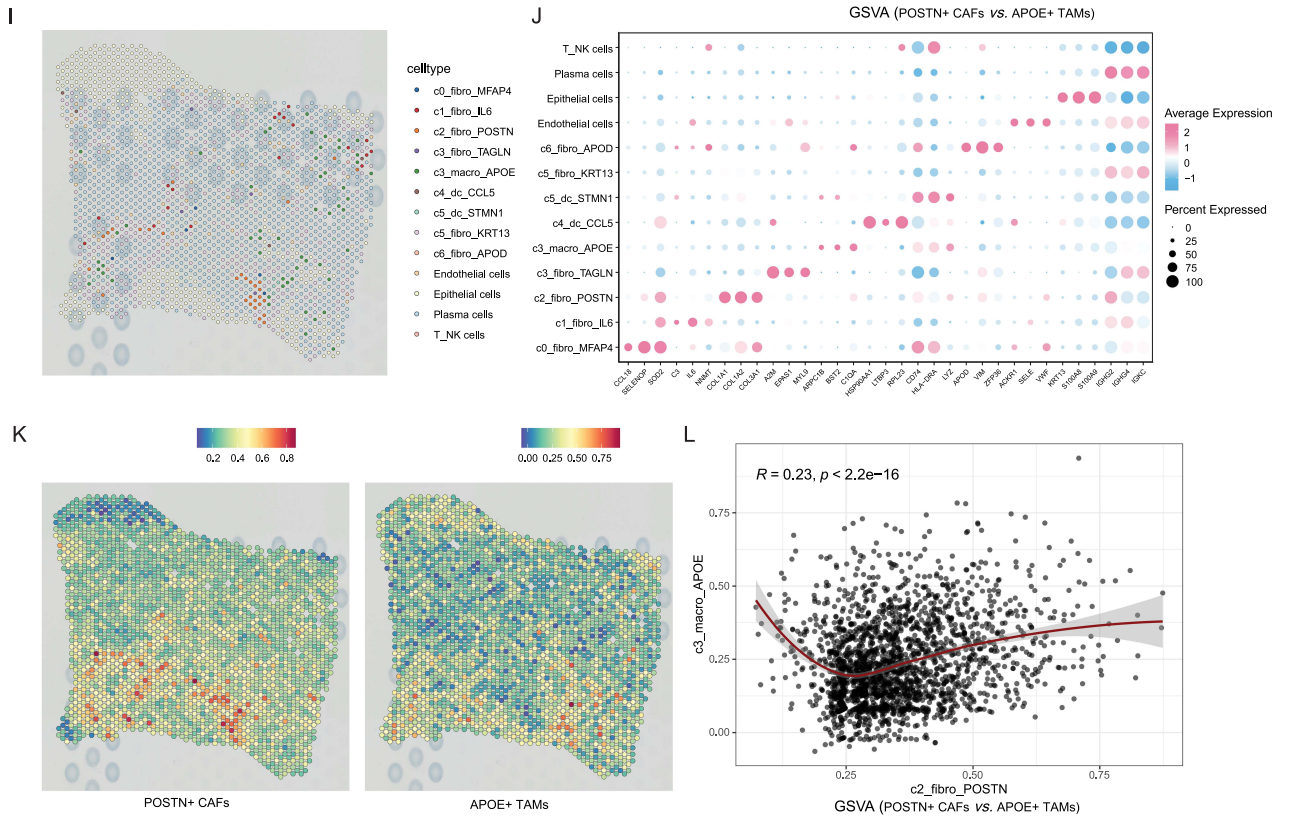

Figure 5 Spatial co-localization and correlation of POSTN$^+$CAFs and APOE$^+$TAMs in HNSC spatial transcriptomics. (**A**–**D**) GSM5494475: spatial mapping of cell subtypes, marker expression, distributions of POSTN$^+$ CAFs and APOE$^+$ TAMs, and their significant correlation. (**E**–**H**) GSM5494476: spatial distribution, marker expression, co-localization, and correlation. (**I**–**L**) GSM5494479: spatial mapping, marker expression, overlapping enrichment, and correlation. All Spearman correlations were significant (all $P < 2.2\times10^{-16}$).

Abbreviations: LSCC, laryngeal squamous cell carcinoma; CAF, cancer-associated fibroblast; TAM, tumor-associated macrophage; HNSC, head and neck squamous cell carcinoma.

Stable Direct Interaction Prediction Between POSTN and APOE Proteins

Based on the evidence of cellular communication and spatial co-localization, we hypothesized that POSTN and APOE may directly interact within the extracellular matrix. Using the HDOCK platform for protein–protein docking, we found that the two proteins fit together very well in terms of shape and space at the binding interface. The best-scoring complex had a docking score of −252.68, which is much lower than the typical score for protein complexes (around −200). This suggests that the interaction is very stable (Figures 7A, Supplementary Table 3).

Electrostatic surface analysis revealed significant charge complementarity, with positively charged areas of POSTN aligning with negatively charged areas of APOE (Figure 7B and C). Electrostatic attraction between acidic residues (Glu, Asp) and basic residues (Lys, Arg) further increased the stability of the complex. The LigPlot$^+$ two-dimensional interaction map showed that residues like POSTN Thr176 and APOE Arg209 were connected by many hydrogen bonds and hydrophobic interactions (Figure 7D).

Collectively, these molecular docking results indicate that POSTN and APOE may form a thermodynamically stable complex through hydrogen bonding, electrostatic, and hydrophobic interactions, providing structural evidence for their synergistic functional cooperation within the LSCC tumor microenvironment.

Co-Enrichment of POSTN$^+$ CAFs and APOE$^+$ TAMs is Strongly Associated with Poor Prognosis

Based on the above findings, we further examined whether the co-enrichment of POSTN$^+$ CAFs and APOE$^+$ TAMs affected patient prognosis. In both TCGA-LSCC and TCGA-HNSC cohorts, patients in the POSTN$^+$ CAFs^{high}/APOE$^+$

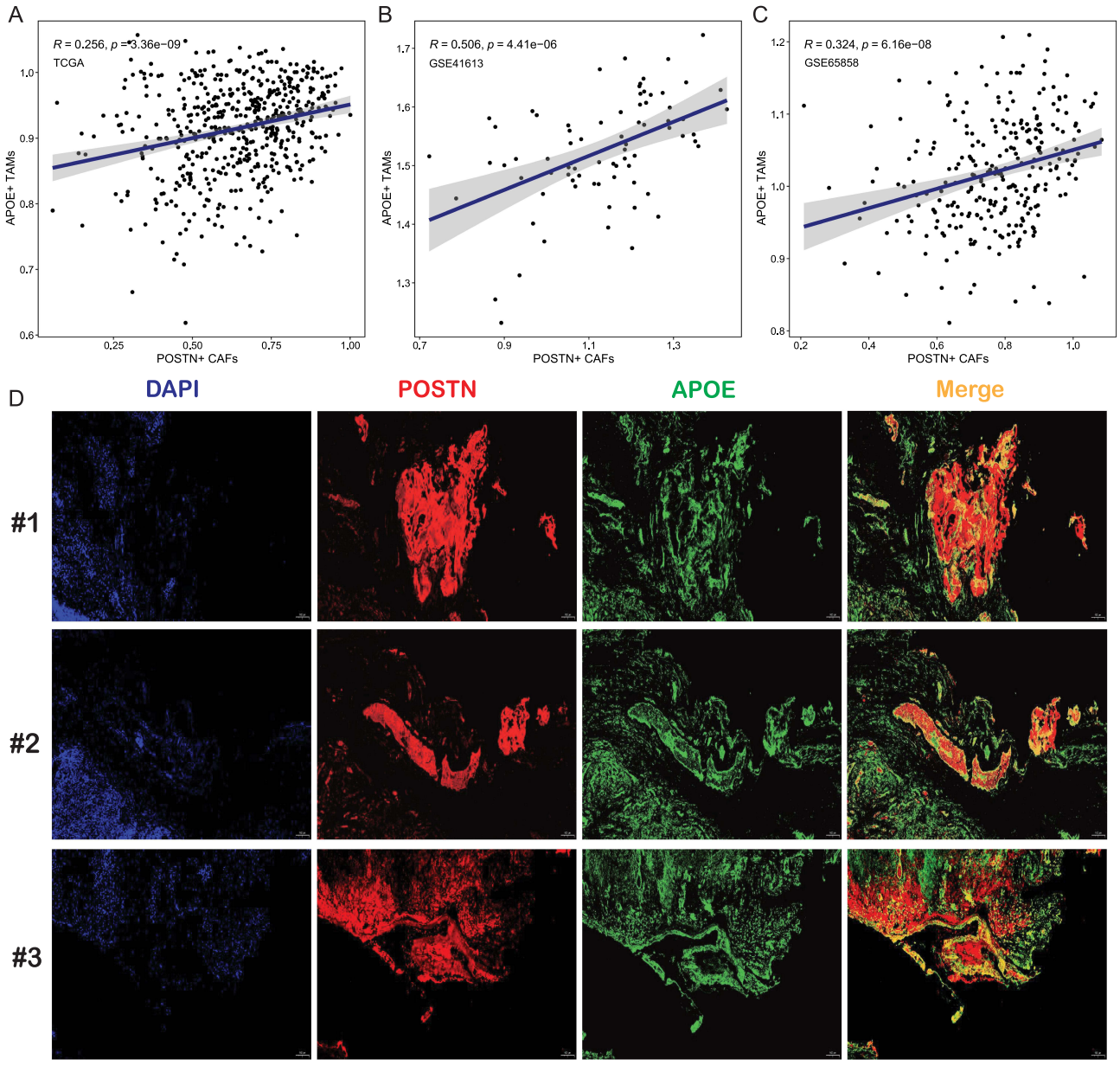

Figure 6 Correlation and spatial colocalization between POSTN$^+$ CAFs and APOE$^+$ TAMs in LSCC. (**A**–**C**) Scatter plots showing the positive correlation between POSTN$^+$ CAF abundance and APOE$^+$ TAM abundance across multiple cohorts, including TCGA-HNSC, GSE41613, and GSE65858. Shaded areas represent 95% confidence intervals, and the correlation was evaluated using Spearman's test. (**D**) Representative multiplex immunofluorescence staining images of LSCC tissues showing colocalization of POSTN (red) and APOE (green) proteins. DAPI (blue) marks cell nuclei.

Abbreviations: LSCC, laryngeal squamous cell carcinoma; CAF, cancer-associated fibroblast; TAM, tumor-associated macrophage; HNSC, head and neck squamous cell carcinoma; DAPI, 4',6-diamidino-2-phenylindole.

TAMs^{high} group had significantly shorter overall survival compared to the POSTN$^+$ CAFs^{low}/APOE$^+$ TAMs^{low} group (Figure 8A, Supplementary Figure 3E).

Functional enrichment analysis comparing POSTN$^+$ CAFs^{high}/APOE$^+$ TAMs^{high} and POSTN$^+$ CAFs^{low}/APOE$^+$ TAMs^{low} groups showed that upregulated genes in the co-enriched group were primarily enriched in biological processes related to extracellular matrix remodeling, such as collagen fibril organization, extracellular matrix structural composition, and collagen metabolic regulation (Figure 8B, Supplementary Figure 3F). Pathway analysis further indicated significant activation of multiple oncogenic pathways, including epithelial–mesenchymal transition (EMT), TGF-β signaling, antigen processing and presentation, and neuroactive ligand–receptor interaction in both TCGA-LSCC and

https://doi.org/10.2147/IJGM.S583478

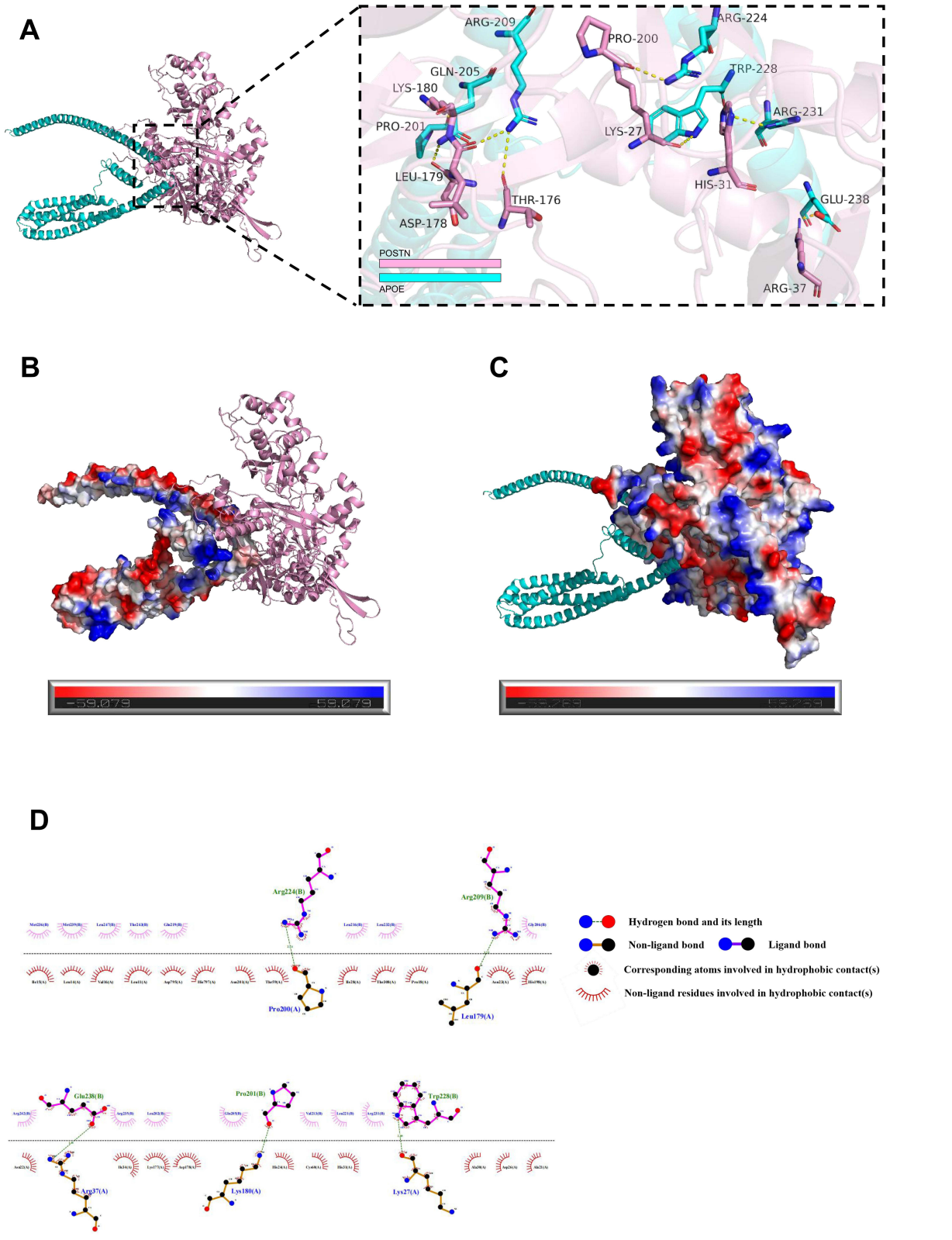

Figure 7 Protein–protein interaction between POSTN and APOE. (**A**) Structural model of the POSTN-APOE complex; the inset highlights key hydrogen-bonding and hydrophobic interactions. (**B** and **C**) Electrostatic potential maps of POSTN (**B**) and APOE (**C**), showing charge complementarity at the interface. (**D**) A 2D interaction diagram illustrating hydrogen bonds and hydrophobic contacts between key residues. Symbols used: red lines for hydrogen bonds, blue circles for non-ligand bonds, and pink arcs for hydrophobic contacts.

Abbreviation: RMSD, Root Mean Square Deviation.

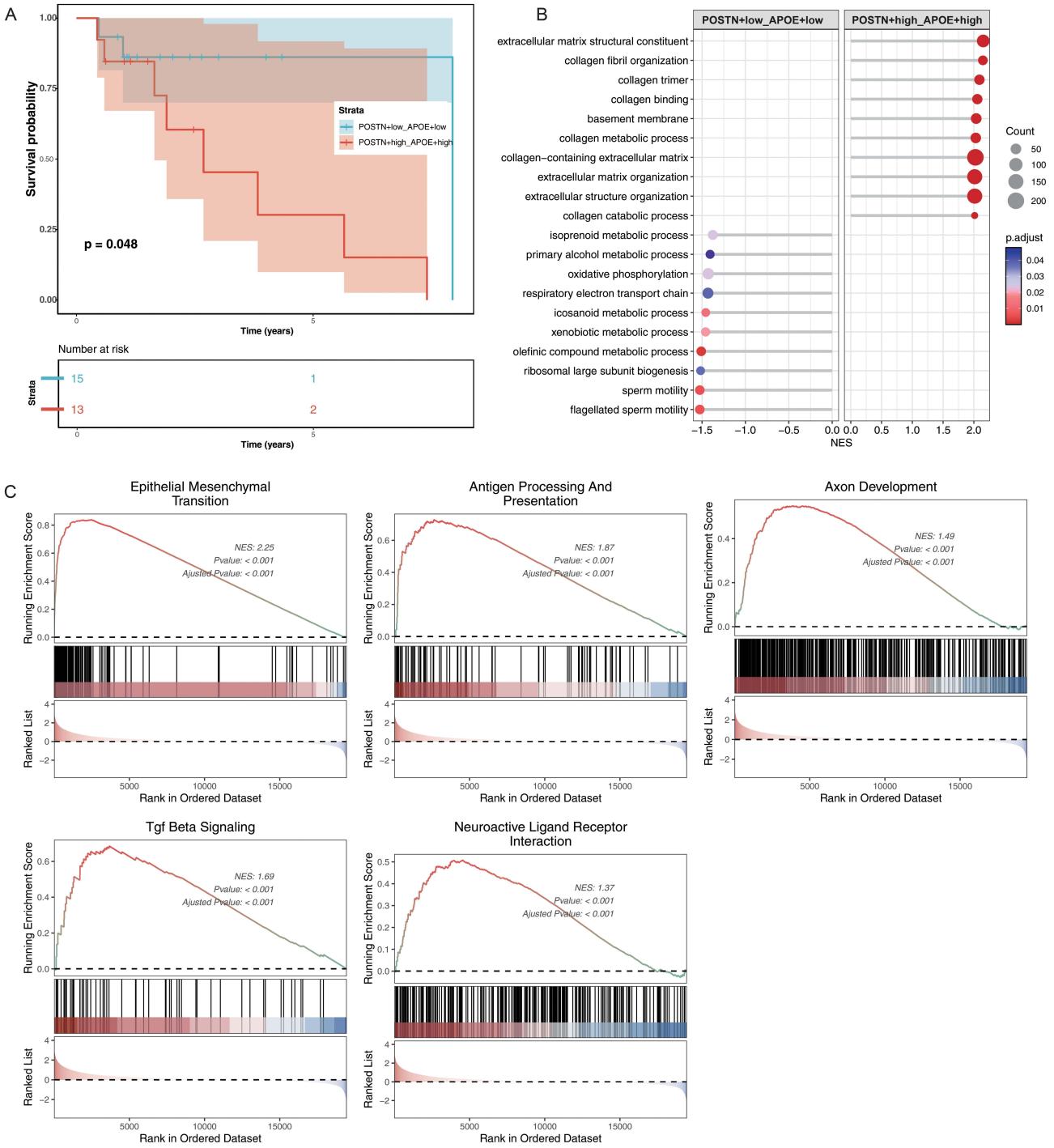

Figure 8 Prognostic and functional implications of POSTN^{+}CAFs and APOE^{+}TAMs co-enrichment. (**A**) Kaplan-Meier survival analysis shows the worst outcomes in the POSTN^{+}CAFs^{high}/APOE^{+}TAMs^{high} group. (**B**) GO analysis reveals enrichment in extracellular matrix organization and collagen regulation in the POSTN^{+}CAFs^{high}/APOE^{+}TAMs^{high} group. (**C**) GSEA indicates activation of EMT, antigen presentation, neuroactive ligand–receptor signaling, and TGF-β pathways in the POSTN^{+}CAFs^{high}/APOE^{+}TAMs^{high} group.

Abbreviations: CAF, cancer-associated fibroblast; TAM, tumor-associated macrophage.

TCGA-HNSC cohorts (Figure 8C, Supplementary Figure 4A). These enriched pathways closely mirror the functional features of POSTN^{+} CAFs, reinforcing their central role in tumor invasion and metastasis via EMT and TGF-β signaling.[40]

https://doi.org/10.2147/IJGM.S583478

Together, these results reveal that co-enrichment of POSTN$^+$ CAFs and APOE$^+$ TAMs not only enhances stromal remodeling and the activation of oncogenic signals but also strongly links with adverse clinicopathologic features, indicating that their synergistic effect could function as a promising prognostic marker and therapeutic target for LSCC.

The POSTN$^+$ CAFs/APOE$^+$ TAMs Axis Shapes an Immunosuppressive Tumor Microenvironment and Predicts Immunotherapy Resistance

To more precisely dissect the influence of POSTN$^+$ CAFs and APOE$^+$ TAMs co-enrichment on the tumor-immune microenvironment, patients were classified into three subgroups based on high (POSTN$^+$ CAFs^{high}/APOE$^+$ TAMs^{high}), intermediate (POSTN$^+$ CAFs^{high}/APOE$^+$ TAMs^{low}, POSTN$^+$ CAFs^{low}/APOE$^+$ TAMs^{high}), or low level (POSTN$^+$ CAFs^{low}/APOE$^+$ TAMs^{low}) of enrichment. Immune cell infiltration was calculated by five deconvolution algorithms (EPIC, MCP-counter, Quanti-seq, TIMER, and ssGSEA). Across all methods, the high group was associated with higher infiltration of various immune cells, including some antitumor populations, compared to the low group (Figure 9A, Supplementary Figure 5). Nevertheless, even with what seems to be an "immune-rich" phenotype, these tumors may also present in a functionally inactivated or "immune-exhausted" state.

Results of ESTIMATE analysis indicated that StromalScore, ImmuneScore, and ESTIMATEScore were significantly higher, whereas Tumor Purity was remarkably lower in the high group, indicating a larger proportion of non-malignant stromal and immune cells within tumor tissue (Figure 9B). We also observed a lower level of immunogenicity and a higher TIDE score in the TCGA-HNSC high group (Supplementary Figure 4B), which might represent a more marked degree of T cell dysfunction and immune escaping, both of which are associated with poor response to immune checkpoint inhibitors (ICIs). These results imply that the POSTN$^+$ CAFs/APOE$^+$ TAMs axis may create an "immune-enriched but immunosuppressed" TME in which immune cell infiltration accompanies defective immune functionality.

These observations were validated in an independent IMvigor210 cohort (urothelial cancer patients who received anti–PD-L1 therapy).[41] Kaplan–Meier overall survival analysis showed a decrease in patients' overall survival with elevated POSTN$^+$ CAFs abundance (p = 0.086; Figure 9C) and APOE$^+$ TAMs abundance (p = 0.044; Figure 9D). Meanwhile, patients with co-enrichment of POSTN$^+$ CAFs and APOE$^+$ TAMs had the worst overall survival (p = 0.022; Figure 9E). Response to treatment analysis indicated that the proportions of patients with progressive disease (PD) or stable disease (SD) were significantly higher in the POSTN$^+$ CAFs^{high}/APOE$^+$ TAMs^{high} group, whereas complete responses (CR) or partial responses (PR) rates were markedly increased for POSTN$^+$ CAFs^{low}/APOE$^+$ TAMs^{low} cases (χ^2-test, p = 0.026; Figure 9F).

Together, these results verified in multiple independent datasets suggest that the POSTN$^+$ CAFs/APOE$^+$ TAMs axis contributes to immune impairment and resistance to immunotherapy, identifying it as a putative predictive biomarker and therapeutic strategy for enhancing the therapeutic response to immunotherapies in LSCC.

The Pro-Tumorigenic Effects of POSTN$^+$ CAFs and APOE$^+$ TAMs are Conserved Across Multiple Cancer Types

To explore whether the cooperative oncogenic effects driven by POSTN$^+$ CAFs and APOE$^+$ TAMs are confined to LSCC or represent a more broadly applicable mechanism, we performed pan-cancer analysis using single-cell RNA sequencing (scRNA-seq) data from 11 solid cancer types, involving a total of 546,787 cells. After strict quality control selection, clustering, and annotation processes, fibroblast and macrophage clusters were analyzed further in depth.

The distinct subset of POSTN highly expressed cells (c0-fibro-POSTN) was also found in the fibroblast cells (Figure 10A). Mapping of the LSCC-originated POSTN$^+$ CAF gene set with UCell scoring on a pan-cancer UMAP showed remarkable high-density enrichment (Figure 10B) and much stronger enrichment in cancerous tissues than normal ones (Figure 10C). Meanwhile, in the macrophage population, we also discovered an APOE highly expressed subcluster (c0-macro-APOE) (Figure 10D), and the UCell scores of this subcluster showed a specific abundance pattern within macrophages (Figure 10E). Slightly differently, this subcluster did not show differences in abundance between tumor and normal tissue (Figure 10F).

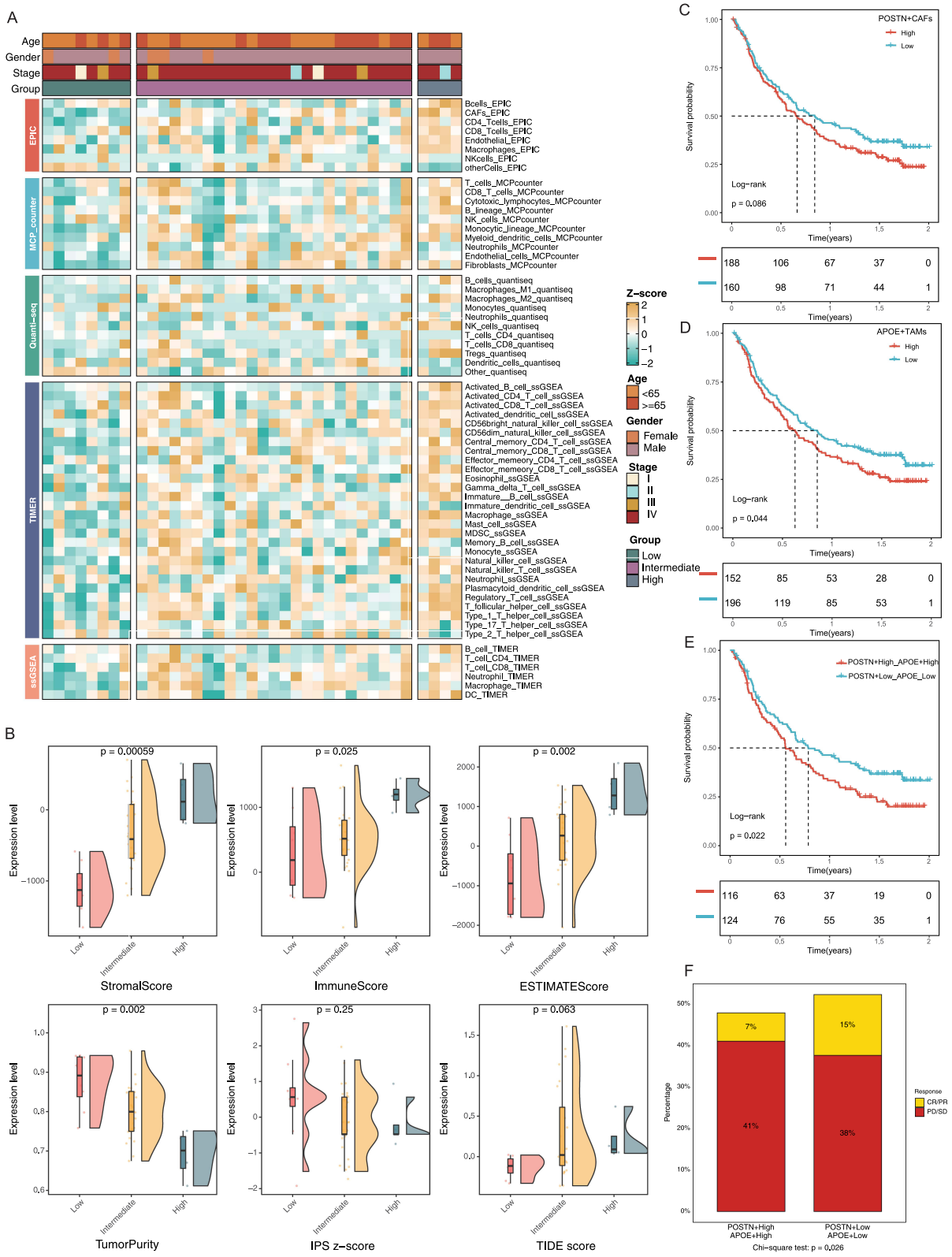

Figure 9 Association of the POSTN^{+}CAFs/APOE^{+}TAMs axis with immune suppression and ICI resistance. (**A**) TME immune cell infiltration across LSCC clinical subgroups quantified by five deconvolution algorithms. (**B**) High POSTN^{+}CAFs/APOE^{+}TAMs enrichment LSCC shows increased stromal and immune scores but reduced tumor purity, as well as TIDE scores with a tendency to be higher. (**C**–**E**) The IMvigor210 cohort validates poorer survival in POSTN^{+}CAFs^{high}/APOE^{+}TAMs^{high} patients. (**F**) Treatment-response comparison shows a higher proportion of PD/SD in the high-risk group (χ^2-test).

Abbreviations: CAF, cancer-associated fibroblast; TAM, tumor-associated macrophage; ICI, immune checkpoint inhibitor; TME, tumor microenvironment.

https://doi.org/10.2147/IJGM.S583478

Further Kaplan–Meier analyses in the TCGA pan-cancer cohort indicated that patients with high abundance of POSTN^{+} CAFs ($p < 0.0001$; Figure 10G) and APOE^{+} TAMs ($p < 0.0001$; Figure 10H) were associated with worse overall survival. When combined, patients in the POSTN^{+} CAFs^{high}/APOE^{+} TAMs^{high} category had the most significant difference relative to the POSTN^{+} CAFs^{low}/APOE^{+} TAMs^{low} category (Figure 10I).

Taken together, these results suggest that the combined pro-tumor effect of POSTN^{+} CAFs and APOE^{+} TAMs is not specific for LSCC but rather universally exists across various solid tumors. This implies a generalized tumor microenvironmental regulatory axis that may promote tumorigenesis, immune escape, and adverse outcomes through the same molecular mechanism.

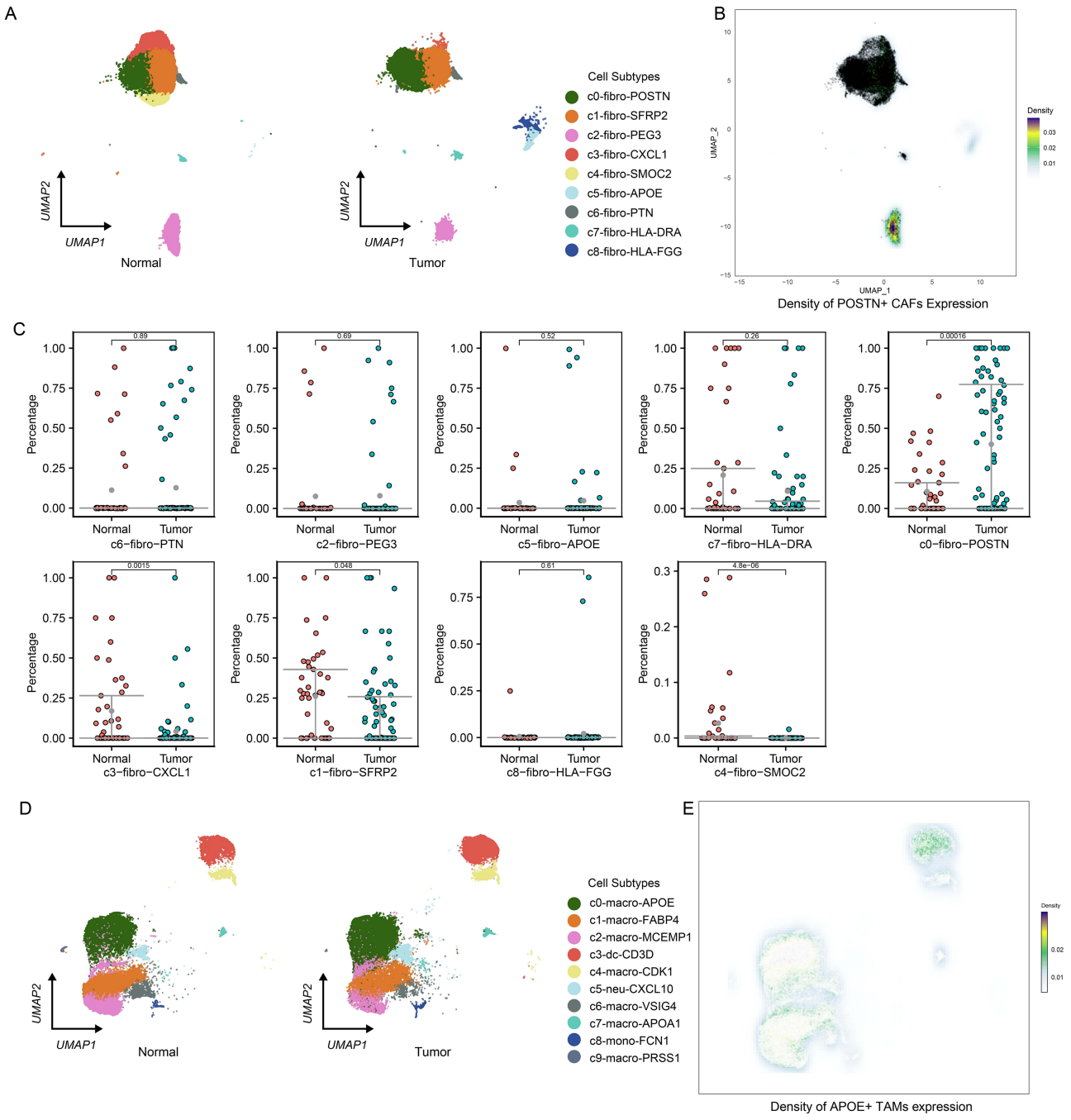

Figure 10 Continued.

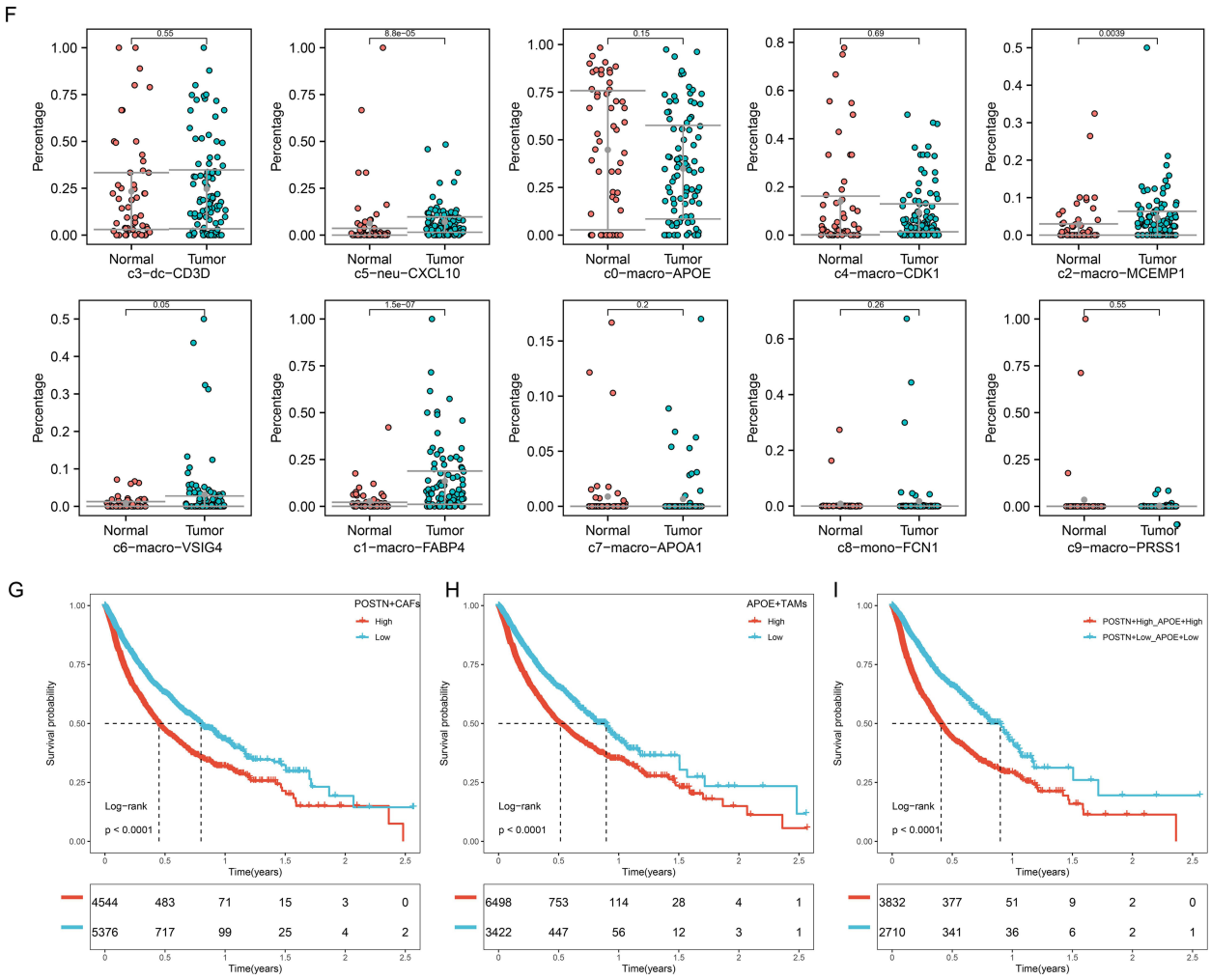

Figure 10 Pan-cancer validation of POSTN$^+$CAFs/APOE$^+$TAMs co-enrichment and prognostic relevance. (**A**) UMAP visualization of fibroblast subclusters across 11 cancer types, with annotations of major subtype identities. (**B**) Density plots of POSTN$^+$CAFs signature scores showing tumor-associated enrichment patterns. (**C**) Comparison of subtype proportions between tumor and normal tissues reveals a significant increase of POSTN$^+$ CAFs in tumors. (**D**) UMAP visualization of macrophage subclusters across 11 cancer types, with annotations of major subtype identities. (**E**) Density plots of APOE$^+$TAMs signature scores showing tumor-associated enrichment patterns. (**F**) Comparison of subtype proportions between tumor and normal tissues reveals a significant increase of APOE$^+$TAMs in tumors. (**G–I**) Pan-cancer survival analyses indicate that high POSTN$^+$CAFs or high APOE$^+$TAMs abundance is associated with poorer overall survival, and patients with POSTN$^+$CAFs^{high}/APOE$^+$TAMs^{high} co-enrichment exhibit the worst prognosis.

Abbreviations: UMAP, Uniform Manifold Approximation and Projection; CAF, cancer-associated fibroblast; TAM, tumor-associated macrophage.

Discussion

In the present study, we systematically described fibroblast and macrophage heterogeneity in the TME of LSCC using multiomics data, including scRNA-seq, spatial transcriptomic, and TCGA bulk RNA-seq datasets. Through our analysis, we revealed the unique enrichment profiles and possible synergistic interplays of POSTN$^+$ CAFs together with APOE$^+$ TAMs. The results showed that both subpopulations were enriched in tumors and were associated with pro-tumorigenic functions such as epithelial–mesenchymal transition (EMT), immunosuppression, etc., leading to a poor clinical prognosis, suggesting that they may serve as key drivers of LSCC malignancy and progression.

POSTN, which is a secreted extracellular matrix (ECM) protein, has been previously reported for its fundamental role in fibrotic diseases and cancer.[18] In tumor biology, POSTN is a well-accepted marker for activated CAFs displaying a myofibroblast-like phenotype (myCAF) [14, 19].[14,19] CAF-produced POSTN promotes ECM remodeling and EMT via paracrine signaling, resulting in increased tumor invasiveness and resistance to therapy.[42] Elevated POSTN expression has been associated with a poor outcome in various types of cancer, such as breast, cervical, and colorectal cancers, as well as esophageal cancer and PDAC.[43] Consistent with these findings, in our study, POSTN$^+$ CAFs in LSCC occupied a

https://doi.org/10.2147/IJGM.S583478

late differentiation stage in pseudotime trajectories and exhibited transcriptomic enrichment in EMT, angiogenesis, and matrix remodeling pathways. TME is often reprogrammed into an immunosuppressive environment during tumorigenesis, which promotes the growth and metastasis of cancer cells.[44] Our findings imply that $POSTN^+$ CAFs might promote the aggressiveness of LSCC by modulating TME. In addition, TCGA survival analysis and pan-cancer validation showed that elevated infiltration of $POSTN^+$ CAFs was an independent risk factor for poor clinical outcomes in various cancer types.

Apolipoprotein E (APOE) is an important secreted glycoprotein mainly produced by hepatocytes and astrocytes and indispensable for cholesterol and lipid homeostasis.[45] In recent years, increasing evidence has highlighted its novel roles in tumor biology.[46] Several other single-cell RNA sequencing (scRNA-seq) studies have revealed an emerging subcluster of APOE-expressing tumor-associated macrophages ($APOE^+$ TAMs) in various types of cancers, including gastric cancer,[47] breast cancer,[48] esophageal squamous cell carcinoma,[49] prostate cancer,[50] colorectal cancer, and lung cancer.[51] $APOE^+$ TAMs are related to M2-like polarization and immunosuppression.[4]

The crosstalk between CAFs and TAMs in the TME is one of the primary factors contributing to the progression of tumors of various types.[52–54] CAF-TAM communication in LSCC is rarely reported. One of the most significant findings of this study is the identification of the synergistic interaction between POSTN+ CAFs and APOE+ TAMs in LSCC. A complex bidirectional signaling network between these two subpopulations was revealed through a cell-cell communication analysis. POSTN+ CAFs possess the ability to secrete cytokines like MIF, which can attract monocytes and trigger their transformation into APOE+ TAMs. Conversely, APOE+ TAMs secrete factors such as NAMPT, which subsequently enhances the activation and survival of CAFs. This positive feedback loop, when combined, creates an immunosuppressive and tumor-permissive environment that is conducive to the progression of LSCC and immune escape. Additionally, spatial transcriptomics verified their in situ co-localization at the cellular level, suggesting direct cell-cell interactions. It is important to note that our protein-protein docking analysis for the first time predicted that a putative interaction between POSTN and APOE proteins could establish a stable complex. This direct binding may enhance the signaling platform in the ECM, stabilize or reinforce mutual signals between CAFs and TAMs, or modulate the TME through a novel molecular mechanism. For instance, the complex that is formed between POSTN and APOE would result in a more robust or long-lasting interaction with cell-surface receptors, thereby facilitating the cooperative regulation of tumor-associated cellular behaviors.

The synergistic interaction of $POSTN^+$ CAFs with $APOE^+$ TAMs has important clinical relevance. Our survival analysis indicated that $POSTN^+$ CAFs/$APOE^+$ TAMs can more precisely predict a poor prognosis in LSCC patients. Meanwhile, we found that their proportion was strongly correlated with the resistance to immunotherapy. Both ESTIMATE and TIDE analyses, along with validation in the IMvigor210 cohort, confirmed that the tumors enriched in these two cell populations contain more obvious immunosuppressive and dysfunctional immune phenotypes and are associated with worse responses to ICI treatment. These observations indicated that the $POSTN^+$ CAFs/$APOE^+$ TAMs axis not only promoted the progress of disease but was also a key factor mediating immune resistance. Thus, targeting this axis through a therapeutic approach may hold promise to avoid treatment resistance. For instance, generation of agents that directly suppress POSTN or APOE activity/interaction may be able to remodel the immunosuppressive tumor microenvironment and sensitize tumors to ICI-based immunotherapy.

Furthermore, our pan-cancer research revealed that the $POSTN^+$ CAFs/$APOE^+$ TAMs axis is not exclusive to LSCC but rather a phenomenon prevalent across other solid tumor types. This discovery significantly broadens the breadth and translational significance of our findings, suggesting that this axis may constitute a conserved and crucial pro-tumorigenic module across many tumor microenvironments. Future research may more rigorously elucidate the molecular foundations and clinical relevance of this axis in other malignancies, which may illuminate the shared principles of tumor-stroma reciprocity and identify novel therapeutic targets within the tumor microenvironment in cancer.

This study has several limitations. First, the analyses were primarily based on retrospective public datasets and computational inference, and therefore the findings should be interpreted as association-based rather than causal. Second, functional validation is currently lacking, and future studies using coculture systems, perturbation experiments, organoid models, and in vivo assays will be necessary to clarify the mechanistic role of the $POSTN^+$ CAF/$APOE^+$ TAM axis in LSCC. Third, the protein–protein docking results provide only theoretical structural predictions and do not confirm direct

physical interaction between POSTN and APOE. Fourth, validation using TCGA-HNSC and the IMvigor210 cohort introduces limitations related to tissue heterogeneity and disease specificity, since these cohorts are not fully equivalent to LSCC-specific validation datasets. Because HNSC comprises anatomically and biologically distinct subsites, validation in TCGA-HNSC should be interpreted as supportive rather than LSCC-specific, and larger LSCC-focused cohorts will be needed to confirm the prognostic relevance of $APOE^+$ TAMs. Finally, the integration of datasets generated from different sequencing platforms, sample sources, and processing workflows may introduce technical and biological heterogeneity. Although the pan-cancer analysis suggests that the $POSTN^+$ CAF/$APOE^+$ TAM signature may recur across multiple solid tumors, the biological consequences of this axis are likely shaped by tumor-specific stromal architecture, inflammatory context, and metabolic constraints.

Conclusion

This study identifies a $POSTN^+$ CAF/$APOE^+$ TAM axis in LSCC that is associated with aggressive clinical behavior, an immune-suppressive tumor microenvironment, and potential immunotherapy non-response, highlighting this axis as a candidate prognostic biomarker and therapeutic target.

Data Sharing Statement

Publicly available datasets were analyzed in this study. Data for single-cell RNA sequencing (scRNA-seq) data and spatial transcriptomics were obtained from the GEO database. Transcriptomic and clinical follow-up data were from The Cancer Genome Atlas (https://xenabrowser.net/datapages/).

Ethics Approval and Consent to Participate

All procedures performed in studies involving human participants were in accordance with the ethical standards of the institutional and/or national research committee and with the 1964 Helsinki Declaration and its later amendments or comparable ethical standards. All tissue specimens were obtained with the consent of the patients themselves and their families, and informed consent forms were signed. The study was approved by the Human Research Ethics Committee of the Affiliated Hospital of Nantong University (No. 2023-K091-01).

Acknowledgments

We acknowledge the resources provided by GEO and TCGA.

Funding

There is no funding to report.

Disclosure

All authors declare no conflicts of interest in the study.

References

1. Gao W, Guo H, Niu M, et al. circPARD3 drives malignant progression and chemoresistance of laryngeal squamous cell carcinoma by inhibiting autophagy through the PRKCI-Akt-mTOR pathway. *Mol Cancer*. 2020;19(1):166. doi:10.1186/s12943-020-01279-2
2. Ma K, Mao Q, Fei B, et al. Metabolic reprogramming and immune microenvironment characteristics in laryngeal carcinoma: advances in immunotherapy. *Front Immunol*. 2025;16:1589243. doi:10.3389/fimmu.2025.1589243
3. Wang Z, Sun A, Yan A, et al. Circular RNA MTCL1 promotes advanced laryngeal squamous cell carcinoma progression by inhibiting C1QBP ubiquitin degradation and mediating beta-catenin activation. *Mol Cancer*. 2022;21(1):92. doi:10.1186/s12943-022-01570-4
4. Liu C, Xie J, Lin B, et al. Pan-cancer single-cell and spatial-resolved profiling reveals the immunosuppressive role of APOE+ macrophages in immune checkpoint inhibitor therapy. *Adv Sci*. 2024;11(23):e2401061. doi:10.1002/advs.202401061
5. Su W, Ling Y, Yang X, Wu Y, Xing C. Tumor microenvironment remodeling after neoadjuvant chemoradiotherapy in local advanced rectal cancer revealed by single-cell RNA sequencing. *J Transl Med*. 2024;22(1):1037. doi:10.1186/s12967-024-05747-x
6. Qin J, Hu S, Chen Y, et al. Hypoxia promotes malignant progression of colorectal cancer by inducing POSTN + cancer-associated fibroblast formation. *Mol Carcinog*. 2025;64(4):716–732. doi:10.1002/mc.23882
7. Chen X, Li W, Lei X, et al. Efficacy of immune checkpoint inhibitors combined with bevacizumab in MSS/pMMR advanced colorectal cancer after first-line treatment failure. *Front Oncol*. 2024;14:1429095. doi:10.3389/fonc.2024.1429095

8. Qin X, Yan M, Zhang J, et al. TGFβ3-mediated induction of Periostin facilitates head and neck cancer growth and is associated with metastasis. *Sci Rep*. 2016;6(1):20587. doi:10.1038/srep20587
9. Yue H, Li W, Chen R, et al. Stromal POSTN induced by TGF-β1 facilitates the migration and invasion of ovarian cancer. *Gynecol Oncol*. 2021;160 (2):530–538. doi:10.1016/j.ygyno.2020.11.026
10. Lei L, Zhang J, Wei R, et al. Deciphering the dual role of autophagy in gastric cancer and gastroesophageal junction cancer: from tumor suppression to cancer progression. *Discov Oncol*. 2025;16(1):1013. doi:10.1007/s12672-025-02802-x
11. Zhao L, Li Q, Zhou T, et al. Role of N6-methyladenosine in tumor neovascularization. *Cell Death Dis*. 2024;15(8):563. doi:10.1038/s41419-024-06931-z
12. Xiong L, Cheng J. Cellular senescence and immunosenescence in melanoma: insights from the tumor microenvironment. *Cancer Med*. 2025;14 (17):e71223. doi:10.1002/cam4.71223
13. Ng M, Borst R, Gacaferi H, et al. A single cell atlas of frozen shoulder capsule identifies features associated with inflammatory fibrosis resolution. *Nat Commun*. 2024;15(1):1394. doi:10.1038/s41467-024-45341-9
14. Wang H, Liang Y, Liu Z, et al. POSTN + cancer-associated fibroblasts determine the efficacy of immunotherapy in hepatocellular carcinoma. *J Immunother Cancer*. 2024;12(7):e008721. doi:10.1136/jitc-2023-008721
15. Micheroli R, Houtman M, Pauli C, et al. OP0102 the synovium in chronic inflammatory joint diseases: comparison of clinical, histological and scRNA-SEQ data between RA, PsA, SpA AND UA. *Ann Rheum Dis*. 2022;81(Suppl 1):67. doi:10.1136/annrheumdis-2022-eular.2773
16. Ma S, Bi W, Liu X, et al. Single-cell sequencing analysis of the db/db mouse hippocampus reveals cell-type-specific insights into the pathobiology of diabetes-associated cognitive dysfunction. *Front Endocrinol*. 2022;13:891039. doi:10.3389/fendo.2022.891039
17. Nie X, Shen C, Tan J, et al. Periostin: a potential therapeutic target for pulmonary hypertension? *Circ Res*. 2020;127(9):1138–1152. doi:10.1161/CIRCRESAHA.120.316943
18. Kanisicak O, Khalil H, Ivey MJ, et al. Genetic lineage tracing defines myofibroblast origin and function in the injured heart. *Nat Commun*. 2016;7 (1):12260. doi:10.1038/ncomms12260
19. Chen C, Guo Q, Liu Y, et al. Single-cell and spatial transcriptomics reveal POSTN + cancer-associated fibroblasts correlated with immune suppression and tumour progression in non-small cell lung cancer. *Clin Transl Med*. 2023;13(12):e1515. doi:10.1002/ctm2.1515
20. Lin S, Zhou M, Cheng L, et al. Exploring the association of POSTN+ cancer-associated fibroblasts with triple-negative breast cancer. *Int J Biol Macromol*. 2024;268(Pt 1):131560. doi:10.1016/j.ijbiomac.2024.131560
21. Kolesnikoff N, Chen C-H, Samuel MS. Interrelationships between the extracellular matrix and the immune microenvironment that govern epithelial tumour progression. *Clin Sci*. 2022;136(5):361–377. doi:10.1042/CS20210679
22. Liu S, Yang S, Zhou X, et al. Nerve injury-induced upregulation of apolipoprotein E in dorsal root ganglion participates in neuropathic pain in male mice. *Neuropharmacology*. 2023;224:109372. doi:10.1016/j.neuropharm.2022.109372
23. Li H, Zhao J, Dai J, et al. Multi-ancestry sequencing-based genome-wide association study of C-reactive protein in 513,273 genomes. *Nat Commun*. 2025;16(1):3892. doi:10.1038/s41467-025-59155-w
24. Hao Y, Hao S, Andersen-Nissen E, et al. Integrated analysis of multimodal single-cell data. *Cell*. 2021;184(13):3573–3587.e29. doi:10.1016/j.cell.2021.04.048
25. Yang S, Corbett SE, Koga Y, et al. Decontamination of ambient RNA in single-cell RNA-seq with DecontX. *Genome Biol*. 2020;21(1):57. doi:10.1186/s13059-020-1950-6
26. Wu T, Hu E, Xu S, et al. clusterProfiler 4.0: a universal enrichment tool for interpreting omics data. *Innovation*. 2021;2(3):100141. doi:10.1016/j.xinn.2021.100141
27. Hanzelmann S, Castelo R, Guinney J. GSVA: gene set variation analysis for microarray and RNA-seq data. *BMC Bioinf*. 2013;14(1):7. doi:10.1186/1471-2105-14-7
28. Trapnell C, Cacchiarelli D, Grimsby J, et al. The dynamics and regulators of cell fate decisions are revealed by pseudotemporal ordering of single cells. *Nat Biotechnol*. 2014;32(4):381–386. doi:10.1038/nbt.2859
29. Jin S, Plikus MV, Nie Q. CellChat for systematic analysis of cell–cell communication from single-cell transcriptomics. *Nat Protoc*. 2025;20 (1):180–219. doi:10.1038/s41596-024-01045-4
30. Kang J, Lee JH, Cha H, et al. Systematic dissection of tumor-normal single-cell ecosystems across a thousand tumors of 30 cancer types. *Nat Commun*. 2024;15(1):4067. doi:10.1038/s41467-024-48310-4
31. Yoshihara K, Shahmoradgoli M, Martinez E, et al. Inferring tumour purity and stromal and immune cell admixture from expression data. *Nat Commun*. 2013;4(1):2612. doi:10.1038/ncomms3612
32. Zeng D, Ye Z, Shen R, et al. IOBR: multi-omics immuno-oncology biological research to decode tumor microenvironment and signatures. *Front Immunol*. 2021;12:687975. doi:10.3389/fimmu.2021.687975
33. Racle J, Gfeller D. EPIC: a tool to estimate the proportions of different cell types from bulk gene expression data. *Methods Mol Biol*. 2020;2120:233–248.
34. Becht E, Giraldo NA, Lacroix L, et al. Estimating the population abundance of tissue-infiltrating immune and stromal cell populations using gene expression. *Genome Biol*. 2016;17(1):218. doi:10.1186/s13059-016-1070-5
35. Finotello F, Mayer C, Plattner C, et al. Molecular and pharmacological modulators of the tumor immune contexture revealed by deconvolution of RNA-seq data. *Genome Med*. 2019;11(1):34. doi:10.1186/s13073-019-0638-6
36. Li B, Severson E, Pignon J-C, et al. Comprehensive analyses of tumor immunity: implications for cancer immunotherapy. *Genome Biol*. 2016;17 (1):174. doi:10.1186/s13059-016-1028-7
37. Fu J, Li K, Zhang W, et al. Large-scale public data reuse to model immunotherapy response and resistance. *Genome Med*. 2020;12(1):21. doi:10.1186/s13073-020-0721-z
38. Xu A, Wang X, Luo J, et al. Overexpressed P75CUX1 promotes EMT in glioma infiltration by activating β-catenin. *Cell Death Dis*. 2021;12 (2):157. doi:10.1038/s41419-021-03424-1
39. Huo R, Zhao R, Li Z, et al. APOE expression in papillary thyroid carcinoma: influencing tumor progression and macrophage polarization. *Immunobiology*. 2024;229(5):152821. doi:10.1016/j.imbio.2024.152821
40. She Z, Chen H, Lin X, Li C, Su J. POSTN regulates fibroblast proliferation and migration in laryngotracheal stenosis through the TGF -β/ RHOA pathway. *Laryngoscope*. 2024;134(9):4078–4087. doi:10.1002/lary.31505

41. Mariathasan S, Turley SJ, Nickles D, et al. TGFβ attenuates tumour response to PD-L1 blockade by contributing to exclusion of T cells. *Nature*. 2018;554(7693):544–548. doi:10.1038/nature25501
42. Chen M, Zheng S-H, Liu Y, Shi J, Qi S-T. Periostin activates pathways involved in epithelial–mesenchymal transition in adamantinomatous craniopharyngioma. *J Neurol Sci*. 2016;360:49–54. doi:10.1016/j.jns.2015.11.042
43. Cao Z, Quazi S, Arora S, et al. Cancer-associated fibroblasts as therapeutic targets for cancer: advances, challenges, and future prospects. *J Biomed Sci*. 2025;32(1):7. doi:10.1186/s12929-024-01099-2
44. Cui X, Li Y, Xie W, et al. Identification of a novel immature dendritic cell subset with potential pro-leukemic effects in leukemia microenvironment. *Cell Death Dis*. 2025;16(1):571. doi:10.1038/s41419-025-07851-2
45. Zhong L, Xie Y-Z, Cao -T-T, et al. A rapid and cost-effective method for genotyping apolipoprotein E gene polymorphism. *Mol Neurodegener*. 2016;11(1):2. doi:10.1186/s13024-016-0069-4
46. Miao G, Zhuo D, Han X, et al. From degenerative disease to malignant tumors: insight to the function of ApoE. *Biomed Pharmacother*. 2023;158:114127. doi:10.1016/j.biopha.2022.114127
47. Liu W, Wang C, Liang L, et al. Single-cell RNA sequencing analysis revealed the immunosuppressive remodeling of tumor-associated macrophages mediated by the MIF-CD74 axis in gastric cancer. *Sci Rep*. 2025;15(1):26883. doi:10.1038/s41598-025-10301-w
48. Xie J, Liu W, Deng X, et al. Paracrine orchestration of tumor microenvironment remodeling induced by GLO1 potentiates lymph node metastasis in breast cancer. *Adv Sci*. 2025;12(32):e00722. doi:10.1002/advs.202500722
49. Jia Y, Zhang B, Zhang C, et al. Single-cell transcriptomic analysis of primary and metastatic tumor ecosystems in esophageal squamous cell carcinoma. *Adv Sci*. 2023;10(7):e2204565. doi:10.1002/advs.202204565
50. Wong HY, Sheng Q, Hesterberg AB, et al. Single cell analysis of cribriform prostate cancer reveals cell intrinsic and tumor microenvironmental pathways of aggressive disease. *Nat Commun*. 2022;13(1):6036. doi:10.1038/s41467-022-33780-1
51. Wei J, Yu W, Chen J, et al. Single-cell and spatial analyses reveal the association between gene expression of glutamine synthetase with the immunosuppressive phenotype of APOE + CTSZ + TAM in cancers. *Mol Oncol*. 2023;17(4):611–628. doi:10.1002/1878-0261.13373
52. Liu L, Wan W, Chang Y, et al. Crosstalk between heterogeneous cancer-associated fibroblast subpopulations and the immune system in breast cancer: key players and promising therapeutic targets. *J Exp Clin Cancer Res*. 2025;44(1):263. doi:10.1186/s13046-025-03527-z
53. Luo M, Zhou L, Huang Z, et al. Antioxidant therapy in cancer: rationale and progress. *Antioxidants*. 2022;11(6).
54. Yan Y, Shi M, Fannin R, et al. Prolonged cadmium exposure alters migration dynamics and increases heterogeneity of human uterine fibroid cells-insights from time lapse analysis. *Biomedicines*. 2022;10(4):917. doi:10.3390/biomedicines10040917